Towards a better rheological investigation of the oxidative aging of bituminous mixes: Frequency versus time characterization

Abderrahim Achchoubi, Sâannibè Ciryle Somé, Ferhat Hammoum, Virginie Mouillet, Jean-François Barthélémy

Towards a better rheological investigation of the oxidative aging of bituminous mixes: Frequency versus time characterization

Abderrahim Achchoubi[1][0009-0001-2873-1767], Saannibè Ciryle Somé[1*][0000-0002-1012-5961], Ferhat Hammoum[2][0000-0001-8449-9707]

Virginie Mouillet[3][0000-0003-2450-9875], Jean-François Barthélémy[1][0000-0002-1968-8939]

[*]ciryle.some@cerema.fr

[1]Cerema, Univ Gustave Eiffel, UMR MCD, F-77171 Sourdun, France
[2]Université Gustave Eiffel, MAST-MIT, Route de Bouaye - CS 5004 - 44344 Bouguenais, France
[3]Cerema, Univ Gustave Eiffel, UMR MCD, F-13100 Aix-en-Provence, France

A B S T R A C T

Aging is among the most common causes of bituminous pavement hardening and engenders premature degradation. The aim of this study is to assess the effect of laboratory aging on the linear viscoelastic properties of bituminous mixes, based on a time and frequency domain characterization, and physicochemical assessment of bituminous concretes and bitumen specimens. It also establishes relationships between the various methods employed. To this end, three thermo-oxidative aging durations (0, 4 and 9 days) have been considered. To simulate the long-term thermo-oxidative aging of binders, RTFOT and PAV tests were conducted on fresh bitumen, followed by physicochemical characterizations (FTIR and asphaltene content) over different aging periods. Tensile creep-recovery and complex modulus tests were also performed to characterize aged and unaged bituminous mixes, in the time and frequency domain respectively. The evolution of axial strain in creep-recovery tests was simulated using calibrated data from the Huet-Sayegh and Generalized Maxwell models in relying on the complex modulus of bituminous concretes and the inverse Laplace transform to switch from the complex to the time domain. These findings show that the stiffness moduli of mixes increase with the duration of long-term thermo-oxidative aging. A number of rheological parameters (R-value, E_c) of bituminous mixes and binders were correlated with aging durations and indices. The evolution of axial strain under creep-recovery conditions provides an instructive relationship between steady-state creep viscosity η_0 and physicochemical parameters, as reflected by a decrease in creep compliance with aging duration and a strong correlation between η_0 and the combined aging index $I_{CO} + I_{SO}$ for all tested temperatures.

Keywords: Thermo-oxidative aging, Creep-recovery, Steady-state creep viscosity, Complex modulus, Physicochemical characterization.

1 Introduction

Across the world, bituminous pavements are used on over 80% of all highways (Zhang et al., 2021). These pavements are composed of different aggregate fractions bound with bitumen. The bituminous mix contains a low proportion of bitumen (generally 5% of the total mass), which nevertheless confers its viscoelastic behavior. The complex internal structure of the bituminous mix, combined with the various environmental and mechanical conditions to which it is subjected, complicates any study of its behavior in road structures.

Bituminous mixes are also subjected to aging effects, from their production through to the final phase of their life cycle. Aging leads to changes in the chemical structure of the binder, which in turn modify

the mechanical properties of the bituminous mix. Gradually over time, as the bituminous binder ages, various properties exhibit distinct alterations: the complex shear modulus and creep stiffness of the binder increase with aging duration, accompanied by a downward trend in both phase angle and unrecoverable creep compliance (Zhang et al., 2018; Wang and Ye, 2020). This evolution of rheological properties has a major impact on the performance of pavements, making them more brittle and increasing their viscosity; moreover, these changes can significantly reduce pavement lifespan and increase the associated repair and maintenance costs. Several studies have identified aging as one of the main factors reducing the durability and performance of bituminous materials (Lu et al., 2011; Fernández-Gómez et al., 2016). The aging process results from a combination of heat, moisture, oxygen and ultraviolet (UV) radiation. The aging of bituminous mixes can be divided into two main phases: short-term aging (STA), and long-term aging (LTA). When bitumen is heated during the production process, oxidation occurs, in affecting its physicochemical characteristics, notably with an increase in polar products, which exert an impact on the material's rheology (Hofko et al., 2017; Zhang et al., 2019; Somé et al., 2022). This initial aging phase, known as STA, arises primarily from the high temperatures (>130°C in the case of hot-mix bitumen) at which bituminous mixes are manufactured, transported, laid and compacted on the construction site, thus leading to volatilization of the lighter bitumen fractions (volatile compounds) when exposed to air. Yet on the other hand, LTA is mainly due to onsite progressive oxidation at ambient temperature, as part of the bituminous mix exposure to environmental agents. In contrast with short-term aging, long-term aging entails a slow oxidation process occurring primarily within the upper few millimeters of the surface layer. In their study, Coons and Wright (1968) found that only the top 12.5 mm of pavements showed significant aging. Contact with oxygen in the air and exposure to ultraviolet rays are the two most important factors affecting the aging of bituminous mixes in service (Durrieu et al., 2007). Other factors also influence the degree of aging, including internal variables like the nature of the bitumen, aggregates, air voids and the bitumen film surrounding the aggregates (Kandhal et al., 1996; Omranian et al., 2018; Mastoras et al., 2021).

For pavement structure design and modeling, the linear viscoelastic characteristics of bituminous mixes constitute a key input. For this reason, it is particularly important to understand the changes in the viscoelastic properties of bituminous mixes caused by aging, as well as characterize them accurately in the laboratory. In order to simulate the *in situ* aging of such mixes and examine the evolution of both the physicochemical and viscoelastic properties of bituminous pavements, a number of laboratory aging protocols have been developed. These methods focus on the aging of the bitumen, loose mixture and compacted specimen (Sirin et al., 2018). Thermo-oxidative aging processes applied to bitumen make use of methodologies such as the Rolling Thin Film Oven (RTFO) (CEN EN 12607-1, 2014) to simulate short-term aging during bitumen manufacturing and Pressure Aging Vessel (PAV) (CEN EN 14769, 2012), which simulates long-term aging over the pavement service life. Some previous studies claim that laboratory aging using RTFO and RTFO-PAV tests corresponds well to aging in the field. Xiao et al. (2015) showed that PAV reproduces aging effects under real-world conditions over a period onsite estimated at between 7 and 10 years. However, the ability of these bitumen aging protocols to replicate onsite aging remains questionable, as these protocols do not account for other aging mechanisms caused by UV radiation or water exposure, which nonetheless occur in situ.

Numerous aging procedures have been documented for bituminous mixes in the existing literature, with dozens of unique methodologies being identified. Note that a selection of these approaches has been standardized in the CEN TS12697-52 guidelines (CEN TS12697-52, 2017), for the purpose of establishing a central framework for the study of bituminous concrete aging in Europe. Noteworthy among these is the RILEM TG5 2009 aging procedure (De La Roche et al., 2009), applied on a loose mixture stored at 135°C for 4 hours, to simulate short-term aging, then cooled to 85°C and placed in a temperature-controlled oven for 9 days before compaction. For compacted specimens, Pierard and

Vanelstrate (2009) proposed an alternative standardized aging protocol. Compared with aging protocols for compacted materials, the aging of loose mixtures offers considerable advantages, including a uniform and homogeneous aging throughout the mixture, as enabled by the ease of circulation of air and heat over the entire material surface. An additional advantage consists of the absence of problems associated with shape change, loss of sample integrity and change in air void distribution caused by the aging of compacted materials (Reed, 2010). However, the aging of loose mixtures is not a perfect procedure. Indeed, the compaction of aged bituminous mixes has often proved to be problematic since the mix becomes too stiff due to the loss of volatile bitumen compounds. Another effective bituminous mix aging process is Viennese Binder Aging (VBA) applied to a loose mixture (Sreeram et al., 2021); this method is based on the VBA method proposed by Mirwald et al. (2020), which offers the novelty of incorporating highly reactive gases (reactive oxygen species (ROS), ozone (O_3) and nitrogen oxides (NO_x)). A new aging procedure for compacted bituminous specimens, called "Viennese Aging Procedure" (VAPro), has recently been developed (Maschauer et al., 2023). This procedure also utilizes a mixture of ROS, O_3 and NO_x to age the samples under conditions similar to those in the field (+ 60°C and pressure < 0.5 bar).

Despite the wide array of laboratory aging methods, an accurate assessment of *in situ* aging and the prediction of the evolution of properties with the aging of bituminous materials used in actual pavements remain questionable and require further investigation. Such predictions are typically based on an examination of specific indicators, often focusing on physicochemical, rheological or mechanical indicators (Lamontagne et al., 2001; Lu et al., 2008; Kambham et al., 2019; Wang et al., 2020; Tabasi et al., 2023). However, very few studies have provided a comprehensive study based on all these parameters. Somé et al. (2023) recently proposed an overview of the effects of thermo-oxidative aging on certain mechanical characteristics of bituminous mixes as well as on the chemo-rheological properties of binders; moreover, these authors suggested correlations between the aging index (AI) and a number of characterized parameters.

The various studies conducted demonstrate that aging induces a modification in the physicochemical and linear viscoelastic properties of asphalt mixes and bitumen. Frequency domain tests providing complex Young's modulus (E^*) or complex shear modulus (G^*) are the most widely used to determine the viscoelastic properties of bituminous materials (Shell Pavement Design, 1978; Guide for mechanistic, 2004; Mohammad, 2014). The application of sinusoidal loads at low strain levels is the simplest way of characterizing the viscoelastic behavior of bituminous mixes over a wide temperature range; for instance, this approach is particularly useful for examining aging effects (Zhang et al., 2022; Briliak et al., 2022; Somé et al., 2022). Typically, complex modulus tests reveal an increase in stiffness with aging, which can be attributed to an increase in asphaltene content, as well as carbonyl and sulfoxide indices at the chemical level.

In addition, or as an alternative to frequency domain tests, it is possible to investigate the aging of asphalt mixes through time domain tests such as creep test, although this type of testing is rarely carried out on asphalt mixes. Creep test is more representative of static loads applied to pavements and yield key parameters for the viscoelastic properties of bituminous materials (Soleimani, 1967). Linear viscoelastic theory demonstrates that the complex modulus can be derived from the creep compliance through a Volterra integral (yielding the relaxation function), followed by a Fourier transform. This theoretically established relationship was recently employed by Daoudi et al. (2020) to demonstrate the consistency between the complex modulus $E^*(\omega)$ results calibrated using the 2S2P1D model, coupled with Kopelman's (1958) and the creep compliance results. Good agreement between the creep compliances predicted from complex modulus $E^*(\omega)$ data and the creep compliance measurement results was observed.

At the binder scale, Hammoum et al. (2009) conducted a study to predict the creep compliance of the Bending Beam Rheometer (BBR) test by using the Prony series obtained from the complex Young's modulus E^* in order to validate the model in the time domain.

In comparison with existing works, this study proposes an alternative method for monitoring the effect of oxidative aging of bituminous mixes by means of creep recovery and complex modulus tests. In parallel, the physicochemical properties of the bitumen have been assessed over different aging periods. Comparisons through correlations across the various methods are drawn in order to highlight their suitability for measuring the effect of oxidative aging. Furthermore, the link between the time domain (creep test) and frequency domain (complex modulus test) is proven by validating the time temperature superposition principle TTSP for the linear viscoelastic parameters of both tests as well as by modeling the creep-recovery test using dynamic modulus data. Additional correlations will be established between the chemical aging indices of binders and rheological properties, on the one hand, and between the chemical indices of binders and the mechanical properties of bituminous mixes (as determined by the creep-recovery test) on the other.

2 Materials and mix design guidelines

2.1 Material properties

The bituminous mixture used in this study is Asphalt Cement 10 (AC 10) (EN13108-1, 2017), which is commonly introduced for surface and binder courses. This mixture is produced with a paving grade bitumen 50/70, featuring needle penetration (EN1426, 2018) and softening temperature properties (EN1427, 2018) of 54 × 0.1 mm and 50°C, respectively, plus porphyry aggregates from the Pont de Colonne quarry. The mix composition and densities of the various constituents are given in Table 1.

Table 1. Mix composition of AC 0/10.

Constituent	Mass content (in %)	Density (in kg m^{-3})
Limestone filler	2.8	2700
0/2	26.10	
2/6.3	24.3	2630
6.3/10	41.4	
Bitumen	5.4	1040

2.2 Thermo-oxidative aging of the bituminous mixes

The protocol applied in this work for aging bituminous mixes was developed based on the European Technical Specification regarding the conditioning methods for bituminous mixes addressing oxidative aging (TS12697-52, 2017). These mixes were all manufactured at 165°C. Once mixed, the loose mixture was cooled to 135°C and spread in a thin layer (up to 2.5 cm) in trays preheated at the conditioning temperature 135°C and placed in a ventilated oven to ensure optimal air circulation around the coated aggregates in order to obtain fast, homogeneous aging. The mix was maintained at 135°C for 4 hours to reproduce short-term aging. Afterwards, specimens were cooled to 85°C and held at this temperature in the oven for 4 or 9 days to simulate long-term thermo-oxidative aging. The mix was then reheated to 135°C for 2 hours and compacted, according to EN 12697-33 (2019), to obtain an aged bituminous concrete slab. A schematic illustration of the mix manufacturing steps and aging durations is shown in Figure 1. The compacted mix without any previous aging serves as the reference and is identified as T0. The mixes subjected to short-term aging for 4 hours and long-term aging have been designated T4, T9 for aging periods of 4 and 9 days, respectively.

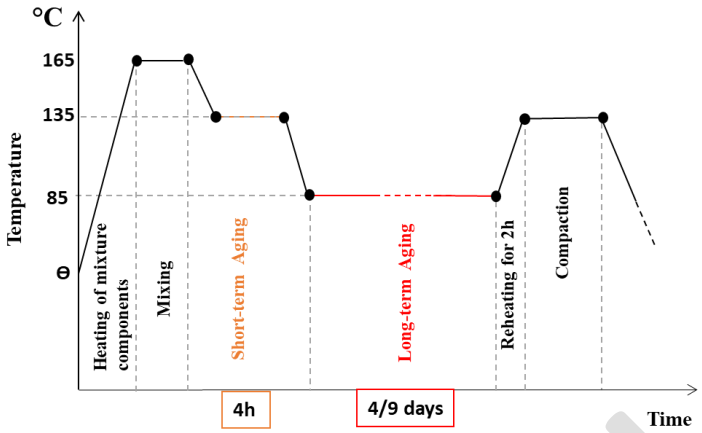

Figure 1. Overview of the manufacturing and aging stages for mixtures.

2.3 Thermo-oxidative aging of bitumen

Bitumen aging was carried out using the RTFOT (rolling thin film oven test) (NF EN 12607-1, 2014) performed at 163°C for 75 minutes to simulate the short-term conditioning. Next, the PAV (Pressure Aging Vessel) (NF EN 14769, 2012) performed at a temperature of 100°C and an air pressure of 2.1 MPa for 20 hours served to mimic the long-term aging. The binders subjected to RTFOT and RTFOT+PAV aging were designated B(RTFOT) and B(RTFOT+PAV) respectively.

Furthermore, the binders were extracted from the aforementioned aged asphalt mixes T0, T4, and T9 then labelled B(T0), B(T4) and B(T9) respectively.

3 Test methods

3.1 2-point cantilever beam test

This test is conducted to determine the complex modulus of bituminous mixes using prismatic specimens 4 × 4 × 12 cm in dimension at temperatures ranging from -20° to 50°C under sinusoidal deflection at four frequencies (from 3 Hz to 40 Hz); it is carried out in accordance with EN 12697-26 (2018) (Annex A: 2PPR). The 2-point cantilever beam test consists of applying, at a given frequency and temperature, a sinusoidal displacement $z = z_0 \times \sin(\omega t)$ on the upper part of a specimen whose base is fixed. The maximum strain applied is limited to 50×10^{-6} m/m, so as to avoid exceeding the linear viscoelastic range of the bituminous mix. The resulting force F and phase angle δ are then measured, to enable calculating the complex modulus $|E^*|$ as per the calculations reported in EN 12697-26 (2018). The master curves can then be constructed from the isotherms of $|E^*|$ and δ (Figures 5 and 6).

3.2 Metravib Dynamic Mechanical Analysis (DMA)

The rheological properties of the virgin and aged bitumen specimens were measured using a Metravib Dynamic Mechanical Analysis (DMA) rheometer, in accordance with FD T66-065 (2018). The complex modulus of bitumen and phase angle δ were measured from 1 to 80 Hz at several temperatures, ranging from -15° to 60°C, in displacement control mode. The bitumen specimens were tested in either shear mode or tension-compression mode. From -15° to 20°C, the tensile-compression tests were conducted on cylindrical specimens 18 mm high and 9 mm in diameter. For temperatures above 20°C, the shear tests were carried out on annular specimens with a shear height of 5 mm, an internal diameter of 8 mm and an external diameter of 10 mm. The measured complex shear modulus $|G^*|$ was converted to $|E^*|$ in considering a Poisson's ratio of 0.5. The isotherms of $|E^*|$ and δ were then used to build the master curves (Figures 8 and 9).

3.3 Conventional bitumen testing

Conventional tests on bitumen were carried out to investigate the various effects of aging; these included the softening point test in accordance with EN1427 (2018), which measures the consistency of bitumen at elevated temperatures, and the penetration test at 25°C in accordance with EN1426 (2018), which determines the material's consistency at ambient temperature.

3.4 FTIR spectroscopy testing on bitumen

The oxygenated species of bitumen, specifically carbonyl and sulfoxide, were quantified using Fourier Transform Infrared (FTIR) spectroscopy. By means of a Perkin Elmer Spectrum 100 FT-IR spectrometer equipped with Spectrum 6.1 software, FTIR spectra recorded in transmission mode could be acquired, with a resolution of 2 cm^{-1} and an accumulation of 32 spectra. This process involves spreading a small quantity of hot bitumen on a transparent plate (KBr), which serves as a transparent support for sample analysis, in line with the recommendations in Mirwald et al. (2022). After recording the FTIR spectrum of the binder, the oxygen species content is determined by measuring the area of the characteristic absorption bands. Given that the consequences of bituminous binder oxidative aging in terms of species formed are now well known (Petersen, 1998), only the carbonyl (with a characteristic infrared absorption band at around 1,700 cm^{-1} (A_{1700})) and sulfoxide (characteristic infrared absorption band at around 1,030 cm^{-1} (A_{1030})) functions are considered (Lamontagne et al., 2001). The experimental procedure detailed in French test method ME69 (Mouillet et al., 2010) was used to measure the oxygenated compounds in this work. The particular procedure is based on the definition of two indices related to carbonyl and sulfoxide functions. This type of approach, known as semi-quantitative infrared analysis, makes it possible to neglect the sample thickness. In applying this approach and assuming that the ethylene (CH_2) and methyl (CH_3) groups, whose infrared bands are located at 1,460 cm^{-1} (A_{1460}) and 1,375 cm^{-1} (A_{1375}) respectively, are not significantly modified by binder oxidation, the two structural indices are calculated as follows:

$$\%I_{CO} = \frac{A_{1700}}{A_{1460} + A_{1375}} \quad ; \quad \%I_{SO} = \frac{A_{1030}}{A_{1460} + A_{1375}} \tag{1}$$

3.5 Creep-recovery test

Creep testing consists of applying a constant, homogeneous load to a specimen under controlled temperature conditions. In this work, a constant tensile force has been applied to a cylindrical specimen for a defined length of time. The mechanical response of the material is expressed by the overall deformation of the specimen, which changes over time. The unloading experiment associated with the creep test is referred to as the recovery. This test is very useful for assessing the viscoelastic behavior of materials (Soleimani, 1967); it involves applying an instantaneous discharge after a constant load has been applied.

Cylindrical specimens measuring 80 mm in diameter and 160 mm high are cored in the horizontal direction of a 400 x 600 x 120 mm slab manufactured in the laboratory. The faces must be perfectly parallel after sawing. Samples are selected according to two criteria: compactness and visual condition (absence of pronounced voids). The samples are bonded to the metal fixtures using a bonding bench for 24 hours. Three pairs of axial extensometers with a gauge length of 25 mm are glued 120° apart from one another to the lateral surface of each specimen in order to measure axial deformations, as seen in Figure 2. Static tensile creep and recovery tests were carried out on aged (4 and 9 days) and unaged bituminous mixes at five different temperatures: -10°C, -5°C, 0°C, 5°C, and 10°C. Before testing,

samples are conditioned at the test temperature for at least 4 hours to guarantee that the fixed temperature inside the specimen is indeed homogeneous. After thermal conditioning, the test protocol consists of applying a tensile force for a defined time (30 seconds), followed by a recovery period. At least three samples were tested for each mix. In order to remain within the domain of linear behavior, limits are imposed on the maximum value of deformation as a function of both the tensile force applied and loading time. The linear viscoelastic limit (LVE) depends on several factors, including the specific type of bitumen, temperature and loading parameters. For frequency domain tests, the LVE is generally set at around 100 µm/m for axial deformation (Airey et al., 2003a; Airey et al., 2003b). For creep tests, Kim et al. (2008) found that LVE reached 450 µm/m at 10°C. In this study, a maximum strain of 130 µm/m was set.

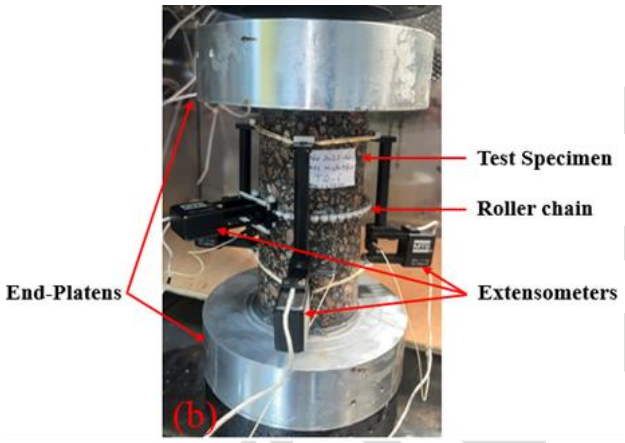

Figure 2. Creep test: (a) overview of hydraulic press; (b) specimen configuration for tensile creep test.

3.6 Master curve construction

The master curve construction process is mainly introduced to standardize the representation of viscoelastic material properties, such as the complex modulus of bituminous materials, by plotting a single curve depicting a spectrum of data recorded at different frequencies and temperatures. The resulting curve provides a global representation of the viscoelastic behavior of bituminous materials, thus enabling a more efficient analysis and prediction of their properties under various conditions. The time-temperature superposition is used to enable shifting the viscoelastic data obtained at different temperatures to a reference temperature by means of shift factors. The method employed to construct master curves is based on the Kramers-Kronig relationship linking the real and imaginary parts of a complex function applied to the complex modulus of bituminous materials, as described in the following studies: Booij et al. (1982), and Chailleux et al. (2006). Isotherms are shifted to derive modulus $|E^*(\omega)|$ and phase-angle $\delta(\omega)$ master curves at the reference temperature T_{ref} = 5°C according to the translation coefficient a (T_i,T_{ref}) calculated using the following equation:

$$\log\left(a_{(T_i,T_{ref})}\right) = \sum_{j=i}^{j=ref} \frac{\log\left(\left|E^*(T_j,\omega)\right|\right) - \log\left(\left|E^*(T_{j+1},\omega)\right|\right)}{\delta_{avr}^{(T_j,T_{j+1})}(\omega)} \cdot \frac{\pi}{2} \quad (2)$$

where $\delta_{avr}^{(T_j,T_{j+1})}(\omega)$ is the average of the phase angles measured at consecutive temperatures T_j and T_{j+1} at the lowest frequency ω, and $\left|E^*(T_j,\omega)\right|$ and $\left|E^*(T_{j+1},\omega)\right|$ are the norms of the complex moduli measured at T_j and T_{j+1} at the lowest frequency ω. Practically speaking, translation coefficients are determined by considering the minimum experimental value obtained for ω and for each isotherm. Using

Equation (2) to calculate translation coefficients makes it possible to adjust coefficients C_1^{ref} and C_2^{ref} of the Williams-Landel-Ferry (WLF) equation as follows:

$$\log\left(a_{(T_i,T_{ref})}\right) = \frac{-C_1^{ref}\left(T_i - T_{ref}\right)}{C_2^{ref} + T_i - T_{ref}} \tag{3}$$

Equation (3) can be written with another reference temperature $T_{ref'}$, in association with other constants $C_1^{ref'}$ and $C_2^{ref'}$, since Equation (3) is independent of the choice of T_{ref} (Ferry, 1980):

$$C_2^{ref'} = C_2^{ref} + T_{ref'} - T_{ref} \tag{4}$$

$$C_1^{ref'} = \frac{C_1^{ref}.C_2^{ref}}{C_2^{ref'}} \tag{5}$$

The complex modulus and phase angle master curve construction method has been implemented in a Python script. This script is designed to generate such master curves based on the data collected from the measurement tests outlined in Sections 3.1 and 3.2.

3.7 Calibration of the rheological model

The present paper has opted for the Generalized Maxwell (GM) model and two special cases of the 2S2P1D model (Olard and Di Benedetto, 2003), namely the Huet-Sayegh model (2S2P) (Sayegh, 1965) and the 1S2P1D model, in order to investigate the complex modulus tests. The GM and 2S2P models have been run to fit the complex modulus results ($|E^*(\omega)|$) of the bituminous mixes, while the 1S2P1D model suffices to fit the $|G^*(\omega)|$ data of the binders.

The GM model, as illustrated in Figure 3, is widely used to describe the viscoelastic behavior of materials across a wider range of frequencies and time scales; it consists of a finite number of Maxwell elements N and an additional spring of stiffness E_0 (not the static modulus of the generalized Maxwell model) Each element corresponds to a relaxation of the material at different time scales. The weighted sum of the stresses applied to each model element equals the overall stress applied to the material. The analytical expression of the GM model for the complex Young's modulus E^* is given by the following equation:

$$E^*(\omega) = E_0 + \sum_{i=1}^{i=N}\left(\frac{E_i.j\omega.\tau_i}{1 + .j\omega.\tau_i}\right) \tag{6}$$

where E_i and $\tau_i = \frac{\eta_i}{E_i}$ represent respectively the i^{th} spring modulus and characteristic time. Here, η_i denotes the viscosity of the i^{th} element, which indeed depends on temperature T.

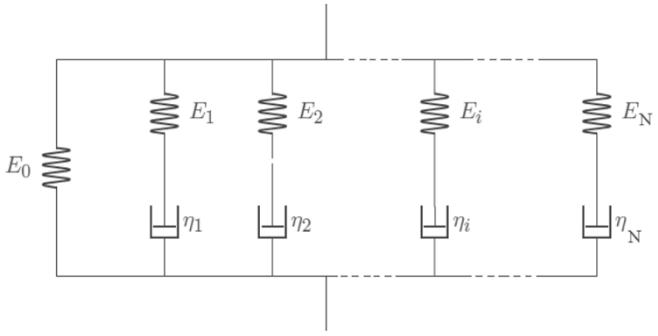

Figure 3. Generalized Maxwell model (GM).

The Huet-Sayegh (HS) model (Sayegh, 1965) has been widely applied to describe the viscoelastic behavior of bituminous mixes. The rheological model consists of a combination of a spring with stiffness E_0 ($E_0 << E_\infty$), connected in parallel to a series of two parabolic elements characterized by parameters h and k ($0 < k < h < 1$) and a spring, as shown in Figure 4. The complex modulus of the HS model is given by:

$$E^*(\omega) = E_0 + \frac{E_\infty - E_0}{1 + \delta(j\omega\tau)^{-k} + (j\omega\tau)^{-h}} \quad (7)$$

In the case of the 1S2P1D model used for binders and based on a combination of 1 spring, 2 parabolic elements and 1 dashpot, characterized by the Newtonian viscosity $\eta = (E_\infty - E_0)\beta\tau$, the E_0 term vanishes from the complex modulus in Equation (7) and a new term appears in the dominator:

$$E^*(\omega) = \frac{E_\infty}{1 + \delta(j\omega\tau)^{-k} + (j\omega\tau)^{-h} + (j\omega\tau\beta)^{-1}} \quad (8)$$

The parameter calibration of the rheological models has been performed using the Subplex optimization algorithm (SBPLX), integrated in the nlopt Python library. This calibration process relies on the results of the phase angle δ vs. reduced frequency ($a_T\omega$) domain. The parameters derived from this optimization step are not unique and moreover depend on the choice of both calibration domain (phase angle δ vs. ($a_T\omega$) domain, Cole-Cole plan, Black space, or E^* vs. ($a_T\,\omega$)) and the optimization algorithm employed.

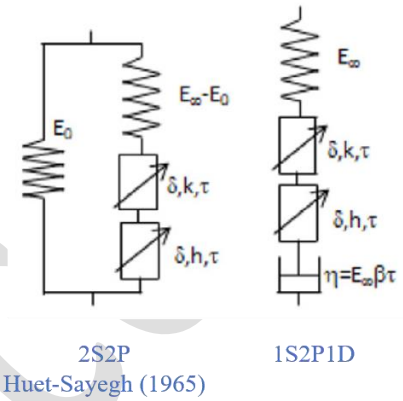

Figure 4. Huet-Sayegh model (2S2P) for mixes and 1S2P1D for binders.

4 Results and Discussion

4.1 Frequency domain characterization of different materials

In order to better understand the influence of different aging levels on the viscoelastic properties of bituminous materials, sinusoidal tests were conducted at various temperatures.

Figures 5 and 6 provide a representation of the raw measurements in the Cole-Cole complex plane and in the Black space. The results in the complex plane reveal a decrease in the loss modulus Im{E} with aging. A slight reduction in the phase angle with aging is also observed in the Black space. To better assess the impact of aging, master curves for the modulus and phase angle are constructed, despite the fact that the curve shifting process may introduce minor errors. The master curves for the complex modulus and phase angle were then plotted using the calculated shift factors a_T. The log(a_T) values for bituminous mixes at a reference temperature of T_{ref} = 5°C are shown in Figure 7 as a function of test temperatures, while the results of the complex modulus and phase angle master curves as a function of aging times are presented in Figures 8 and 9. Curve results reveal a number of trends in the viscoelastic

properties of the tested mixes, in relation to the duration of oxidative aging in the laboratory. As aging time increases, the stiffness moduli of the mixes also increase, whereas the phase angles, which reflect the relaxation capacity of the mixes, decrease. At high frequencies, the stiffness moduli of aged mixes actually tend towards a horizontal asymptote. In fact, at high frequencies, bituminous concrete exhibits more and more elastic behavior, making the effects of aging less noticeable in the log-log representation. These figures also show that the increase in stiffness modulus $|E^*|$ and decrease in phase angle δ are very significant between the reference material T0 and the 4-day aged material T4, yet become small between the 4 and 9-day aged specimens T4 and T9. This finding means that the variation in rheological properties, in particular stiffness modulus $|E^*|$ and phase angle δ, becomes weak when the long-term aging time reaches a certain duration. Several discussions on the optimal temperature to adopt for aging have been held, leading to the adoption of long-term aging at 135°C (Braham et al., 2009; Dukatz et al., 2015), since aging at higher temperatures is more efficient than at lower temperatures (Kim et al., 2018). However, higher aging temperatures can lead to a different type of aging than that observed on actual pavements, due to the disruption of polar molecular associations and the resulting thermal decomposition of sulfoxides in bituminous binders. Rad et al. (2017) drew a comparison between long-term laboratory aging at 95°C and at 135°C, in demonstrating that chemical changes induced by aging at 135°C can have a negative impact on bituminous mix performance, in terms of dynamic modulus values and fatigue resistance.

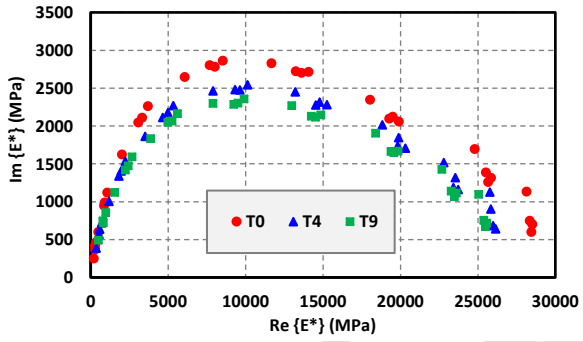

Figure 5. Cole-Cole representation of complex moduli of bituminous mixes.

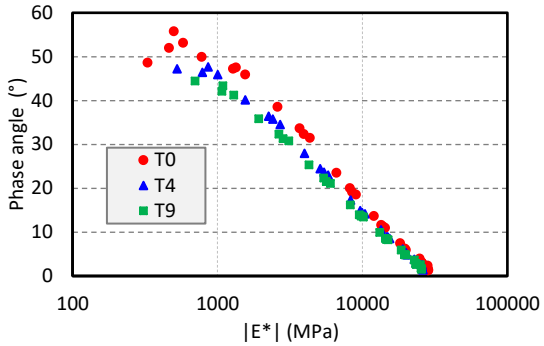

Figure 6. Black space representation of bituminous mixes.

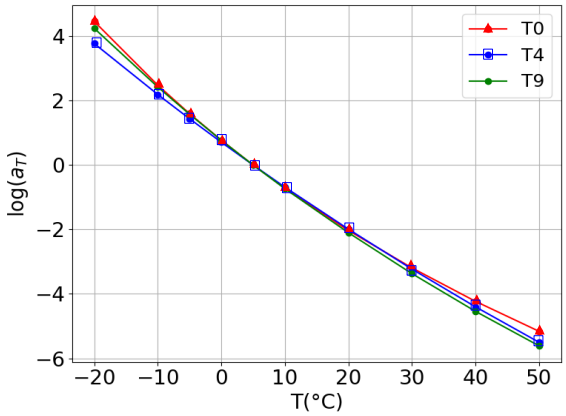

Figure 7. Log(a_T) values for bituminous mixes at T_{ref} = 5°C versus temperature.

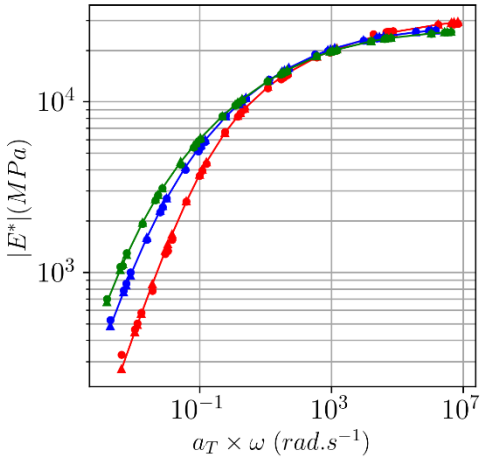

Figure 8. Master curves of complex moduli of bituminous mixes at T_{ref} = 5°C.

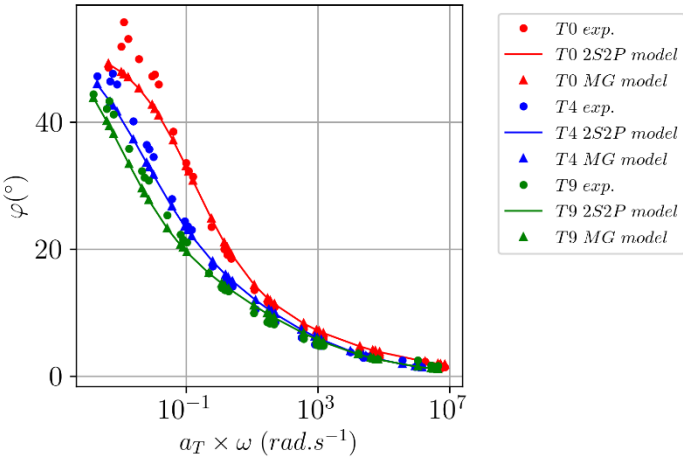

Figure 9. Master curves of phase angle of bituminous mixes at T_{ref} = 5°C.

Similarly, to Figures 5 and 6, Figures 10 and 11 depict a representation of the raw measurements in the Cole-Cole complex plane and in the Black space. The results in the complex plane reveal a decrease in the loss modulus Im{E} with aging. A slight reduction in the phase angle with aging is also observed in the Black space, consistent with the observations made on bituminous binders (Figures 5 and 6).

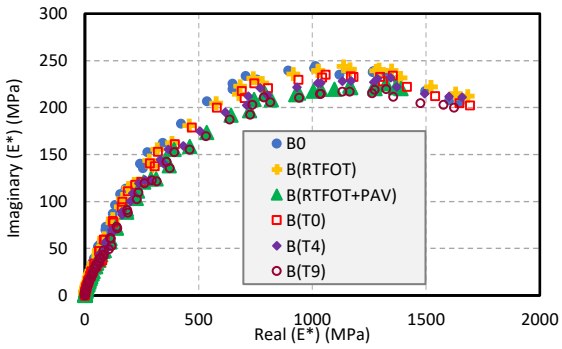

Figure 10. Cole-Cole representation of complex moduli of bitumens.

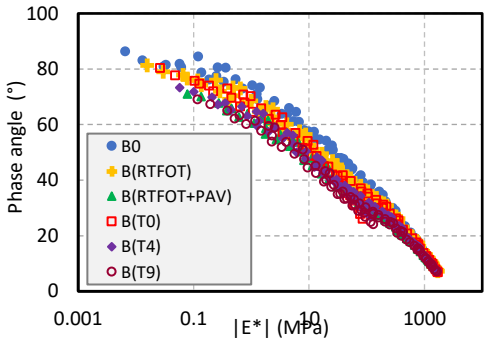

Figure 11. Black space representation of bitumens.

The complex modulus and phase angle master curves for both virgin and recovered bitumen specimens are plotted in Figures 12 and 13. As for bituminous mixes, the effect of aging on the viscoelastic properties of bitumen is clearly perceptible. Similarly, the bitumen complex modulus $|E^*|$ increases with long-term oxidative aging duration, thus leading to a decrease in their phase angles δ. As shown in Figures 12 and 13, the master curves for extracted bitumen B(T0) and bitumen aged with RTFOT run very close, confirming that RTFOT successfully simulates short-term bitumen conditioning, as previously demonstrated in the literature (Mollenhauer et al., 2011). RTFOT at 163°C + PAV aging procedure appears to have a lesser impact on binder properties than RILEM's 9-day long-term aging procedure on loose mixes, which in turn leads to a greater increase in shear complex modulus. Mollenhauer and Mouillet (2011) reported that application of the PAV method for 20 hours at 90°C and a pressure of 2.1 MPa yields a level of aging similar to that of loose mixes aged for 9 days at 85°C. Other studies have revealed that chemical and rheological changes are not always consistent. As a result, the aging sensitivity of binders can be classified differently according to the evaluation method employed (Lu and Isacsson, 2002). Previous works have already studied the effect of aging on bituminous mixes and bitumen, reaching the same conclusions as those presented below (Braham et al.,

2009; Yang et al., 2018; Crucho et al., 2020; Somé et al., 2022). The increase in complex modulus vs. aging time has been proven to be one of the most obvious indicators of the effect of aging.

The results of the complex modulus tests have been modeled using the Generalized Maxwell (GM) and Huet-Sayegh (2S2P) models for bituminous mixes and 1S2P1D model for binders. As shown in Figures 8, 9, 12 and 13, the calibration produced is indeed accurate. The parameters obtained from this process are presented in Tables 2 and 3 for the modified 2S2P1D models and in Table 4 for the GM model. The rheological parameters of these models can be used as aging process indicators (Somé et al., 2022). The data listed in Table 2 indicate that for E_{∞}, k and h held constant, the shape parameter δ and characteristic time τ increase with the long-term aging duration. Table 3 lists the parameters for bituminous binders modeled with the 1S2P1D model. The Newtonian viscosity constant β, as well as the shape parameter δ and characteristic time τ, show an increasing trend with aging time.

It should be noted that it would have been possible to use the 2S2P1D model for both bitumen and asphalt mixes, which would allow for the comparison of the parameters of each extracted bitumen with those of the corresponding aged asphalt mix. However, the authors have chosen to use the model with the minimum number of parameters that allows for fitting the curves of the bitumen on one hand and those of the asphalt mixes on the other hand. This leads to the choice of the 2S2P model for asphalt mixes and the 1S2P1D model for bitumen.

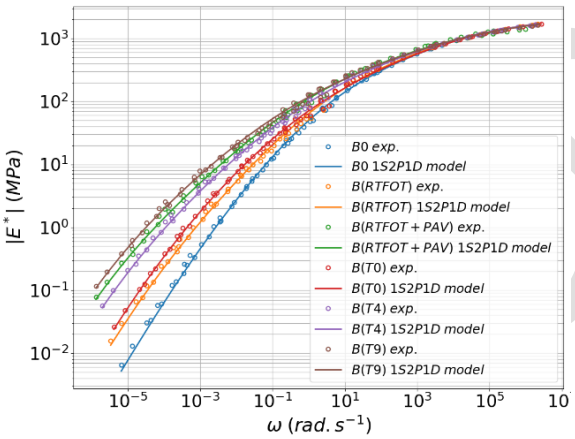

Figure 12. Master curves of complex moduli of binders at T_{ref} = 5°C.

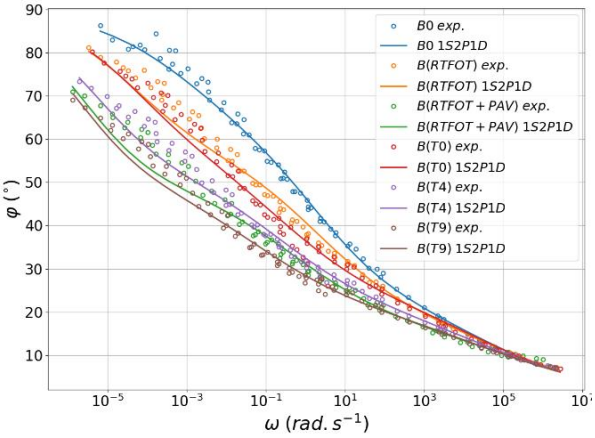

Figure 13. Master curves of phase angle of binders at T_{ref} = 5°C.

Table 2. Huet-Sayegh (2S2P) model parameters for bituminous mixes at T_{ref} = 5 °C.

Mixes	E_0 (MPa)	E_∞	δ	τ	k	h	-	C_1	C_2
T_0	23	25 000	3.06	9.38	0.3	0.67	-	22.5	151.5
T_4	60	25 000	4.62	26.49	0.3	0.67	-	45.2	325.0
T_9	10	25 000	6.139	96.41	0.29	0.67	-	32.8	218.3

Table 3. 1S2P1D model parameters for bitumens at T_{ref} = 5 °C.

Bitumen	E_∞	δ	τ	k	h	β	C_1	C_2
B_0	2400	2.83	$1.55e^{-03}$	0.24	0.57	222.1	24	115.3
$B_{(RTFOT\ 163)}$	2400	3.43	$3.04e^{-03}$	0.24	0.57	650.3	26.5	126.4
$B_{(RTFOT\ 163+PAV)}$	2400	5.97	$2.91e^{-02}$	0.24	0.57	1420	43.8	265.6
$B(T_0)$	2400	4.29	$5.36e^{-03}$	0.24	0.57	562.2	24.1	110.7
$B(T_4)$	2400	5.37	$1.64e^{-02}$	0.24	0.57	1069	30.4	153.5
$B(T_9)$	2400	7.21	$5.40e^{-02}$	0.24	0.57	1239	30.8	151.5

Figures 14 and 15 illustrate respectively the effect of long-term thermo-oxidative aging on the characteristic time τ and shape parameter δ of the rheological models 2S2P and 1S2P1D. It can be observed that the values of the shape parameter δ of the recovered binders are higher than those of bituminous mixes. In addition to the gradual increase in these parameters, the τ values for these mixes are over 1,000 times greater than the τ values for the recovered binders. Although the bituminous mixes and recovered binders have been subjected to the same aging protocol, such a difference in the characteristic time values would be expected and is mainly explained by the presence of aggregates in the mixes. This outcome also affects the choice of appropriate rheological model for each material (2S2P for the mixes and 1S2P1D for bitumen), as well as the boundary conditions imposed on model parameters during the optimization process.

Table 4. Generalized Maxwell model parameters for bituminous mixes at T_{ref} = 5 °C.

T_0		T_4		T_9	
Ei (MPa)	τi (s)	Ei (MPa)	τi (s)	Ei (MPa)	τi (s)
9.63 e^{01}	-	1.19e^{02}	-	1.93e^{02}	-
7.24e^{02}	4.61e^{-07}	9.16e^{02}	8.13e^{-07}	9.77e^{02}	4.73e^{-07}
4.74e^{02}	1.62e^{-06}	7.18e^{02}	2.75e^{-06}	1.12e^{03}	3.27e^{-06}
9.92e^{02}	5.70e^{-06}	4.44e^{02}	9.30e^{-06}	1.28e^{03}	2.03e^{-05}
9.52e^{02}	2.01e^{-05}	1.47e^{03}	3.14e^{-05}	1.93e^{03}	1.23e^{-04}
1.34e^{03}	7.06e^{-05}	7.82e^{02}	1.06e^{-04}	2.13e^{03}	9.46e^{-04}
8.63e^{02}	2.49e^{-04}	1.56e^{03}	3.59e^{-04}	2.20e^{03}	5.19e^{-03}
2.16e^{03}	8.75e^{-04}	1.54e^{03}	1.21e^{-03}	2.22e^{03}	2.69e^{-02}
1.89e^{03}	3.08e^{-03}	1.53e^{03}	4.11e^{-03}	2.38e^{03}	1.24e^{-01}
2.11e^{03}	1.08e^{-02}	2.15e^{03}	1.39e^{-02}	2.72e^{03}	6.91e^{-01}
1.78e^{03}	3.81e^{-02}	1.56e^{03}	4.70e^{-02}	2.46e^{03}	3.69
2.65e^{03}	1.34e^{-01}	2.38e^{03}	1.59e^{-01}	2.23e^{03}	1.79e^{01}
2.31e^{03}	4.72e^{-01}	1.68e^{03}	5.37e^{-01}	1.83e^{03}	7.91e^{01}
2.26e^{03}	1.66	2.13e^{03}	1.81	1.29e^{03}	3.35e^{02}
2.40e^{03}	5.84	2.00e^{03}	6.14	7.63e^{02}	1.46e^{03}
2.35e^{03}	2.06e^{01}	1.73e^{03}	2.07e^{01}	4.33e^{02}	7.56e^{03}
1.69e^{03}	7.24e^{01}	1.59e^{03}	7.03e^{01}		
1.07e^{03}	2.55e^{02}	1.04e^{03}	2.37e^{02}		
4.30e^{02}	8.96e^{02}	6.72e^{02}	8.03e^{02}		
1.89e^{02}	3.15e^{03}	3.13e^{02}	2.71e^{03}		
9.16e^{01}	1.11e^{04}	2.34e^{02}	9.19e^{03}		

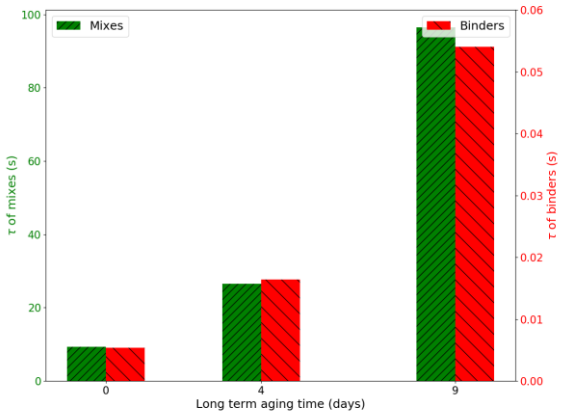

Figure 14. Evolution of the characteristic time τ of mixes and binders with aging (2S2P and 1S2P1D models).

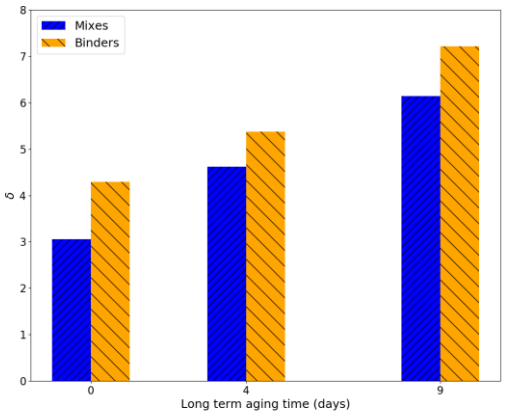

Figure 15. Evolution of the shape parameter δ of mixes and binders with aging (2S2P and 1S2P1D models).

The parameters of the Generalized Maxwell model provided in Table 4 are used to construct the relaxation spectra for better visualization of the different relaxation modes E_i associated with each characteristic time τ_i, as well as the contribution of each mode E_i to the mechanical response of the binders (Figure 16). A unimodal distribution of Ei as a function of τ_i is observed. The relaxation times exhibit a very broad spectrum, ranging from 10^{-7} to 10^{4} seconds. The extensive range of the spectrum (numerous τ values) indicates that aged binders exhibit a multimodal behavior, characterized by complex viscoelastic contributions.

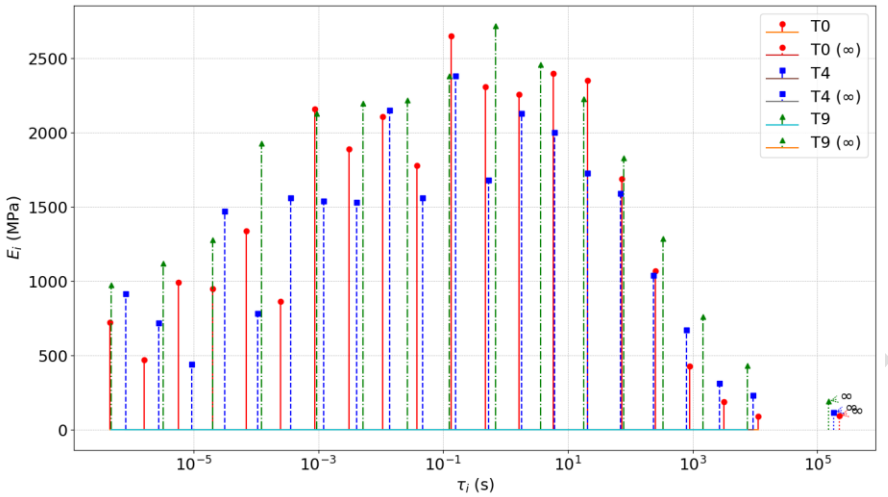

Figure 16. Relaxation spectra of bituminous mixes at T_{ref} = 5 °C.

4.2 Effect of aging on the physicochemical properties of bitumen

Figure 17 displays the FTIR spectra of the aged binders and the most significant changes occurring on the spectra, merely a section between 1800 and 500 cm^{-1} is shown. The physicochemical characteristics of bitumen are listed in Table 5. The mean values of the carbonyl $I_{C=O}$ and sulfoxide $I_{S=O}$ indices are calculated based on three repeatability measurements. An increase in carbonyl $I_{C=O}$ and sulfoxide $I_{S=O}$ indices is observed during thermo-oxidative aging, leading to a gradual decrease in penetrability and an increase in softening temperature. When considering the sum of carbonyl $I_{C=O}$ and sulfoxide $I_{S=O}$ indices, a combined aging index AI = I_{CO} + I_{SO} is obtained. AI increases gradually from 3% for fresh bitumen (B0) to 9.6% for bitumen recovered from T0, then to 14.1% for bitumen recovered from T4, and finally to 18.7% for bitumen recovered from T9. A higher asphaltene content is also noticeable in aged binders. On the basis of I_{CO}, I_{SO} and asphaltene content, the aging conditions of T9 mixes appear to be more aggressive than those of the RTFOT+PAV binder protocol; this observation is in agreement with previous findings (Somé et al., 2022).

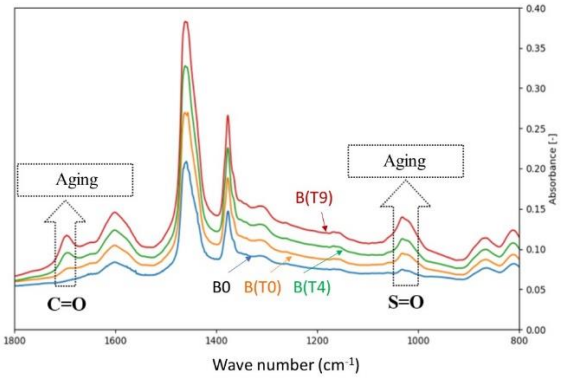

Figure 17. FITR Spectra of aged bitumen

Table 5. Physico-chemical properties of aged bitumens.

Bitumen	$I_{C=O}$ (%)	$I_{S=O}$ (%)	$I_{C=O}+I_{S=O}$	Asphaltene (%)	Pen (0.1 mm)	T_{RB} (°C)
B0	0 ± 0.5	3 ± 0.5	3	12.1	54 ± 0.7	50 ± 0.7
$B(RTFOT\ 163)$	0.2 ± 0.5	4 ± 0.5	4.2	14.1	32 ± 0.7	56 ± 0.7
$B(RTFOT\ 163 + PAV)$	3.1 ± 0.5	11 ± 0.5	14.1	17.6	19 ± 0.7	65.8 ± 0.7
B(T0)	1.2 ± 0.5	8.4 ± 0.5	9.6	15.3	29 ± 0.7	57.2 ± 0.7
B(T4)	3.9 ± 0.5	10.2 ± 0.5	14.1	17.2	21 ± 0.7	64.4 ± 0.7
B(T9)	4.7 ± 0.5	14 ± 0.5	18.7	19.9	13 ± 0.7	69.2 ± 0.7

4.3 Creep-recovery test

The complete creep curve for viscoelastic materials, such as asphalt mixtures, generally exhibits three distinct regimes: a primary creep phase corresponding to the quasi-instantaneous response of the material, followed by a stage during which the strain rate $\dot{\varepsilon}(t)$ decreases non-linearly over time due to the relaxation of internal stresses. The secondary phase is characterized by a constant or stabilized average strain rate $\dot{\varepsilon}(t)$, which appears as a plateau on the $\dot{\varepsilon}(t)$ graph. In the tertiary phase, $\dot{\varepsilon}(t)$ increases rapidly due to mechanisms such as material damage (e.g., cracking, cavitation) and changes in the internal structure of the material.

For the purposes of this study, we focus exclusively on the secondary creep phase, during which the steady-state viscosity can be determined.

The applied force and axial strain for a creep-recovery test on a sample of unaged bituminous mixes at 5°C are plotted in Figure 18. It is clearly shown that axial strain rises during the loading period and that creep behavior can be divided into primary creep and steady-state creep stages.

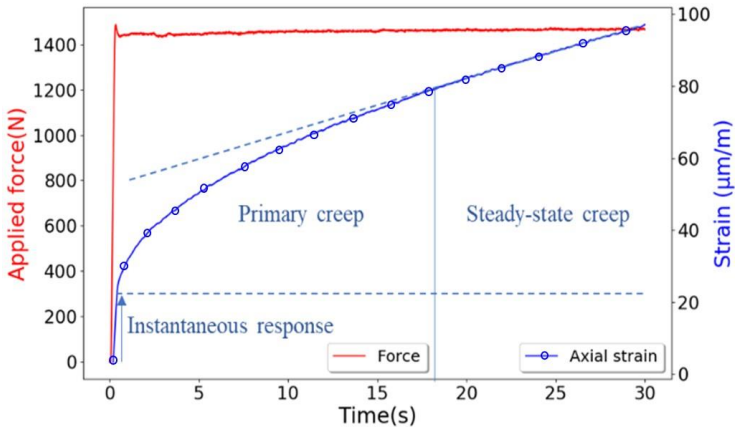

Figure 18. Applied force and axial strain for uniaxial tensile creep test at 5°C for mix T0.

For the experimental tests, the applied forces given in Table 6 are chosen according to the test temperature, so as to ensure that the maximum deformation is not exceeded (130 µm/m). The range of force to be applied has been defined based on three criteria: i) A maximum deformation criterion of 130 µm/m, which should not be exceeded to remain within the linear domain. For this, we refer to the work of Kim et al. (2008), which indicates that linearity is ensured up to 450 µm/m at 10°C in tensile test on asphalt mixtures. ii) A significant deformation level compatible with the precision of the extensometers used for measuring deformations. iii) A sufficient force level compatible with the precision of the force sensor of the hydraulic press used. Indeed, it is not recommended to measure forces below 1 kN with the press being used. Applied stresses may vary slightly due to small geometric disparities measured between specimens. In order to avoid any slight differences in stress levels that may occur between different tests, the static creep compliance J(t) was computed; this parameter is defined for the loading period in Equation (9) as the evolution of axial strain as a function of time $\varepsilon_1(t)$ under the application of a constant stress σ_{01}. The concept of homogeneity in linear viscoelasticity theory states that the relationship between strain response and any applied stress remains independent of the magnitude of the stress.

$$J(t) = \frac{\varepsilon_1(t)}{\sigma_{01}} \tag{9}$$

Creep-recovery curves for T0, T4 and T9 mixes at the various test temperatures (-10°C, -5°C, 0°C, 5°C and 10°C) are presented in Figure 19. It can be seen from this figure that the creep-recovery compliance of the mixes is sensitive to temperature change. At low temperatures (-10°C, -5°C, 0°C), creep compliance variations are relatively small; however, as temperatures rise to positive values, the sensitivity to temperature becomes significantly more pronounced, resulting in more blatant differences in creep behavior. In the recovery region shown in the second half of the curve, the elastic deformation disappears instantaneously, while the delayed deformation shapes the recovery phase. Yet the time set for recovery, limited here to 100 seconds, is insufficient to attain the total recoverable deformation, especially at 10°C. For other temperatures, the deformations reached at the end of the recovery are very low (less than 20 µm/m), which lies within the accuracy limits of strain measurement by extensometers, hence allowing us to consider that total recovery has been reached.

Table 6. Test conditions for creep recovery tensile test

Temperature (°C)	-10	-5	0	5	10
Applied force (N)	2000	1500	1500	1500	1000
Stress (MPa)	0.4	0.3	0.3	0.3	0.2

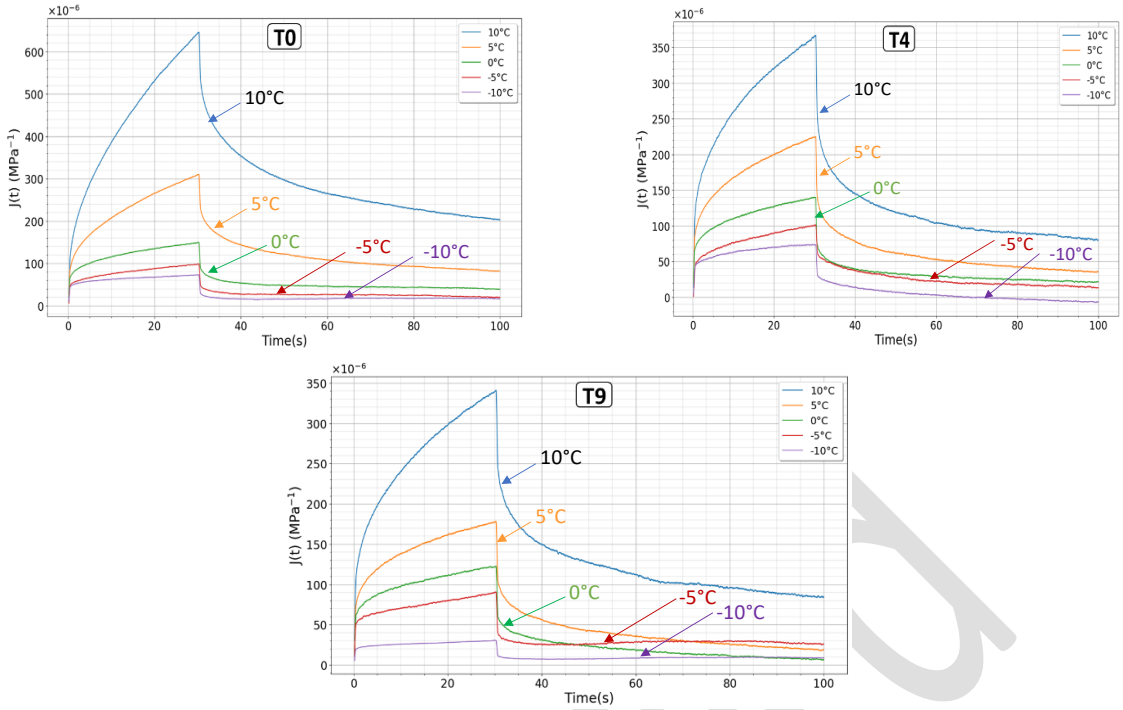

Figure 19. Creep-recovery curves of AC 0/10 T0, T4 and T9 at different temperatures.

4.4 Creep compliance master curves

In this section, the results obtained from the creep-recovery test are used to construct the creep compliance master curves for both the aged and unaged bituminous mixes, as displayed in Figure 20. An efficient approach to determining the shift factors involves visually adjusting the creep curve at different temperatures in order to generate a smooth creep compliance master curve. However, employing this manual shifting method might induce errors during the construction process. Various studies (Buttlar et al., 1998; Witczak et al., 2000) have recommended an automated procedure for generating the creep compliance master curve to avoid visual errors. The shift factors (a_T) used in this paper are the same as those employed when constructing the master curves of dynamic modulus, which were shown in the log(a_T) versus temperature curves (see Figure 7). The time-temperature superposition can then be validated for the creep test performed on both aged and unaged bituminous mixes. Note that this parallel shift factor for both frequency (dynamic modulus test) and time domains (creep test) implies a robust correlation between the material's viscoelastic response under various experimental set-ups. Such concordance underscores the consistency of the material's response within different test domains, thus reinforcing the effectiveness of time-temperature superposition as a tool for understanding and modeling the behavior of bituminous mixes under different conditions.

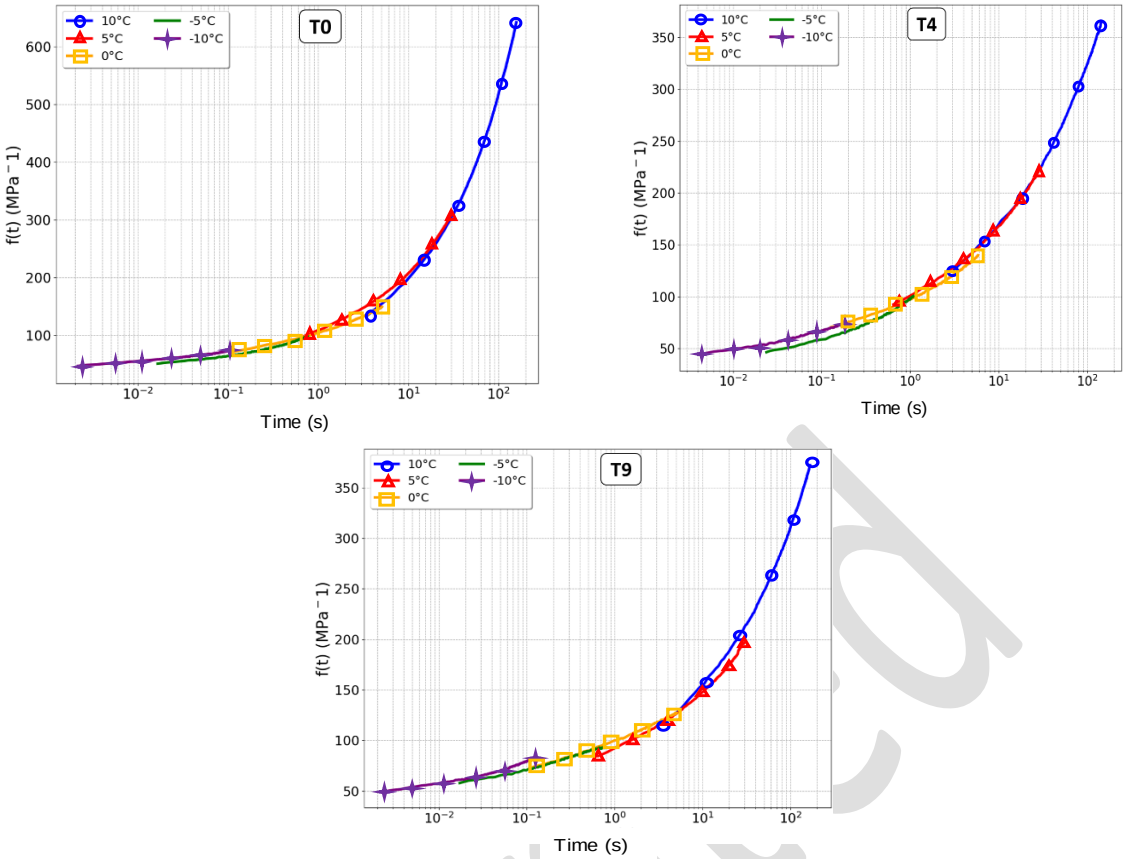

Figure 20. Master curves of tensile creep compliances for AC 0/10 T0, T4 and T9 at Tref=5°C.

4.5 Creep-recovery modeling using complex modulus data for bituminous mixes

In order to simulate creep behavior, we have used calibrated data from both the 2S2P and Generalized Maxwell models, based on experimental results for the complex modulus of bituminous mixes.
The complex modulus represents the amplitude of the harmonic response generated by the complex deformation when placed under a steady-state stress condition, as expressed in Equation (10):

$$\varepsilon^*(i\omega) = \varepsilon_0 e^{i\omega t} \quad \sigma^*(i\omega) = E^*(i\omega)\,\varepsilon_0\, e^{i\omega t} \tag{10}$$

Although both models are widely used to study the behavior of viscoelastic materials under various conditions, neither provides an exact analytical creep compliance function. Some authors have proposed procedures for approximating creep compliance in order to overcome this challenge. Nguyen et al. (2022) approximated the compressive creep compliance computed numerically by the sum of exponential functions. In this paper, the Laplace transforms $\mathcal{L}$ method has been used to convert time domain functions into functions of a complex variable. The inverse Laplace transform, denoted $\mathcal{L}^{-1}$, refers to the conversion of functions from the complex domain back to the time domain.

The definition of the Laplace-Carson transform for any function such that $f(t<0)=0$ is as follows:

$$f^*(p) = \mathrm{p}\mathcal{L}\{f\}(p) = p\int_{t=-\infty}^{+\infty} e^{-pt} f(t)dt = \int_{t=-\infty}^{+\infty} e^{-pt} f'(t)dt \tag{11}$$

Applying the Laplace-Carson transform to the linear viscoelastic behavior of bituminous material gives the following elastic-like equation:

$$E^*(p) = \frac{\sigma^*(p)}{\varepsilon^*(p)} \tag{12}$$

Where $\sigma^*(p) = \text{p}\mathcal{L}\{\sigma\}(p)$ and $\varepsilon^*(p) = \text{p}\mathcal{L}\{\varepsilon\}(p)$ are respectively the Laplace-Carson transforms of σ and ε.

Hence the complex modulus is defined by:

$$E^*(i\omega) = E^*(p)|_{p=i\omega} \tag{13}$$

For the creep test defined by the imposed stress:

$$\sigma(t) = \sigma_0 H(t) \tag{14}$$

Where σ_0 is a constant and H is the Heaviside function.

Both the Generalized Maxwell and Huet-Sayegh creep responses can be determined by applying the inverse Laplace transform $\mathcal{L}^{-1}$:

$$J(t) = \mathcal{L}^{-1}\left\{\frac{\varepsilon^*(p)}{p\sigma_0}\right\} = \mathcal{L}^{-1}\left\{\frac{1}{pE^*(p)}\right\} \tag{15}$$

Practically, the invert Laplace was computed numerically using the Cohen (Cohen, 2007) method implemented in the Mpmath Python library.

The recovery test corresponds to a stress-step loading $\sigma(t) = \sigma_0(H(t) - H(t-t_1))$ of duration t_1. Invoking the linearity of the considered viscoelastic behavior, the strain can be written under the following form:

$$\varepsilon(t) = \sigma_0\big(J(t) - J(t - t_1)\big) \tag{16}$$

It is worth noting that the use of the Generalized Kelvin-Voigt model would have been more relevant, as it allows for the determination of the creep function without numerical inversion. However, the Generalized Maxwell model was used in this article because the work presented here is only a part of a broader program, which includes multiscale modeling and finite element analysis (not presented here), where the Maxwell model was more appropriate.

Figure 21 shows a comparison between experimental data and the modeled creep-recovery curve using the 2S2P and GM models for bituminous mixes T0, T4 and T9. It can be noted that the model results generally agree well with the experimental findings for each aging time at all test temperatures. The discrepancies between numerical simulation and experimental results may be due to measurement errors, depending on the precision of the test used to determine the complex modulus of bituminous mixes, as well as to an error, albeit minor, in determining the rheological model parameters. However, these errors remain very slight, not exceeding a few micrometers per meter, as shown in Figure 21, which does not alter the model accuracy. The error between numerical and experimental deformations is minimized thanks to the limit established for the maximum deformation in the creep test; this feature ensures that the behavior remains overall within the linear viscoelastic domain and moreover limits or cancels out any error related to the material viscoplasticity not considered by the model. At higher temperatures, Nguyen et al. (2021) noted a lack of agreement between the creep test and their proposed simulation; their explanation invoked the fact that measured creep deformation actually includes both viscoelastic and viscoplastic deformations at these temperatures (>40°C). Consequently, the measured deformation is not purely viscoelastic; furthermore, significant errors in the creep compliance calculation based on creep test data will occur if the temperature is sufficiently high.

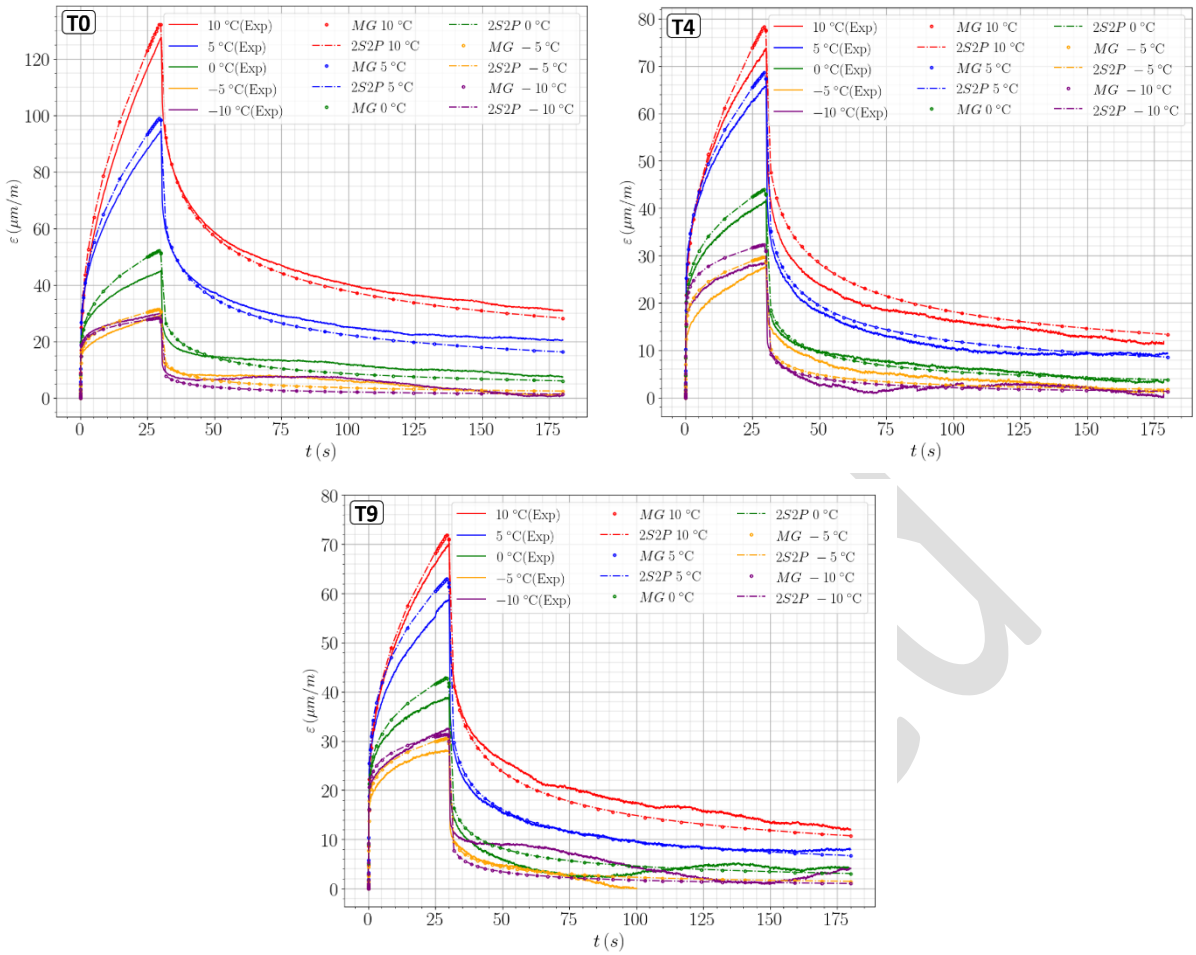

Figure 21. Tensile creep-recovery test at different aging period: Comparison between experimental results and numerical calculation.

4.6 Effect of aging on tensile creep-recovery compliance

The aim of this section is to compare the creep-recovery behavior of bituminous mixes at different aging levels. Creep-recovery curves for T0, T4 and T9 at 10°C, 5°C, 0°C and -5°C are shown in Figures 22 (a) through (d), respectively. It can be observed that aging has a significant impact on the viscoelastic properties measured by the tensile creep-recovery test. The initial compliances J_0 of the three mixes are relatively similar. With a longer aging time, axial creep strain decreases and maximum compliance J_{max} becomes smaller. These same observations in terms of creep strain evolution can be made for the recovery phase. At negative temperature, compliance decreases to low levels during recovery, which corresponds to very small strains that are difficult to measure with precision, leading to fluctuations in the strain measurements, as seen in the creep-recovery region at -5°C (Figure 22 (d)).

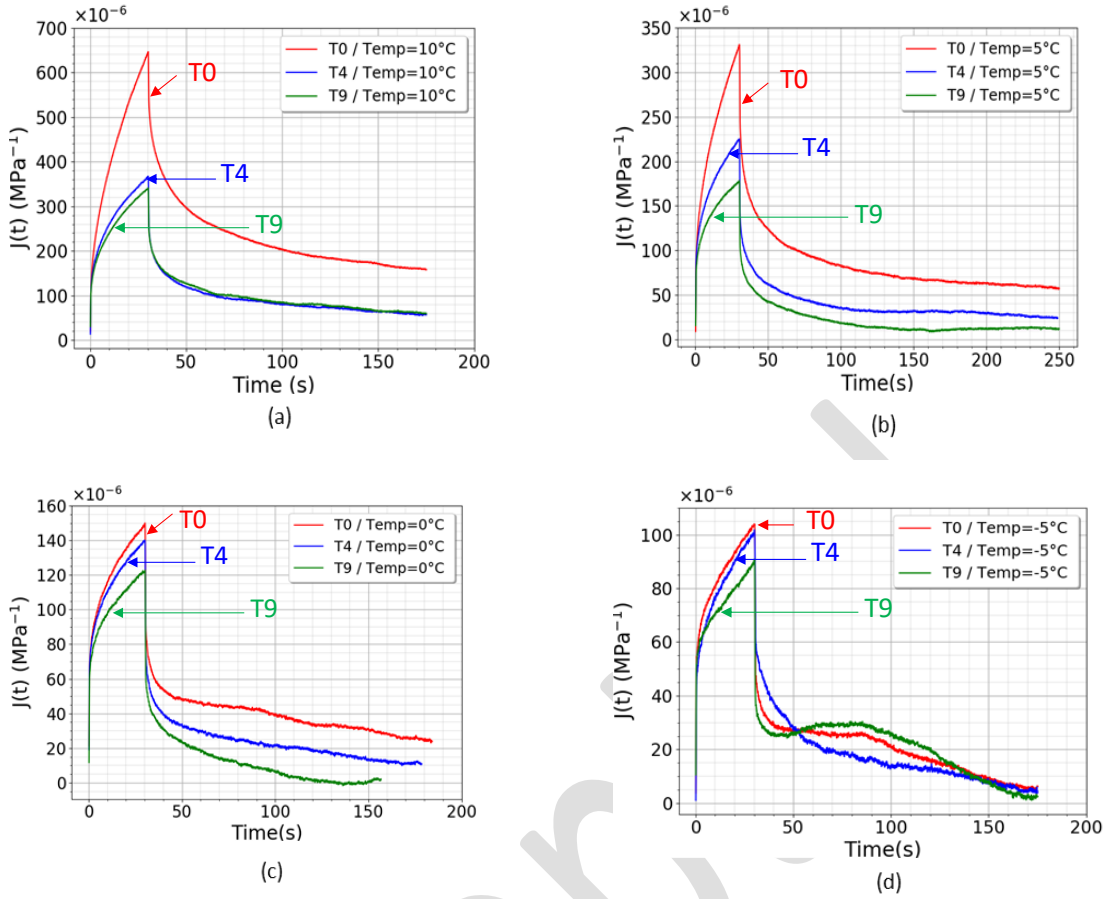

Figure 22. Effect of oxidative aging one the creep-recovery behavior at (a) 10°C, (b) 5°C, (c) 0°C and (d) -5°C.

4.7 Relationship between aging index and mechanical properties

This section assesses the potential link both between the aging effect and mechanical properties characterized in both frequency and time domain.

Some rheological parameters have been selected to characterize both bituminous mixes and binders during laboratory aging processes. These include the crossover modulus E_c corresponding to the crossover frequency ω_c when the phase angle equals 45°, as well as when the storage modulus equals the loss modulus. The crossover modulus has been presented as a useful aging index for studying the evolution of oxidative aging of bituminous binders; in addition, correlations have been established based on this rheological index (Farrar et al., 2013; Glaser et al., 2013; Wen et al., 2016). In the case of thermo-rheologically simple asphalt binders, the crossover modulus is temperature-independent (Gross, 1953; Farrar et al., 2013).

Another rheological index widely used to assess aging is the R-value (Christensen et al., 1992; Margaritis et al., 2020); it describes the relationship between crossover modulus and glass modulus. The R-value for bitumen and bituminous mix is defined in Equation (17):

$$R = \log\left(\left|E_g^*\right|\right) - \log(|E_c^*|) \tag{17}$$

Lesueur et al. (1997) proposed a correlation between the R-value and the total amount of colloidal matter in the bituminous binders. The R-value is directly correlated with bitumen performance, with lower R-values reflecting better mechanical performance (Maschauer et al., 2023).

Below, a relationship between the thermo-oxidative aging index I_{CO} + I_{SO} and the rheological indicators (crossover properties and R-value) of aged mixes and binders is shown. Figures 23 and 24 illustrate the results of the crossover modulus E_c for bitumen and bituminous mix as a function of the combined aging index I_{SO} + I_{CO}. These results reveal that E_c decreases as the aging index I_{CO} + I_{SO} increases for both the mixes and the bitumen. A good linear correlation for the mixes, R^2=1, and a negative correlation between the cross modulus of bitumen E_c vs. aging index can be observed.

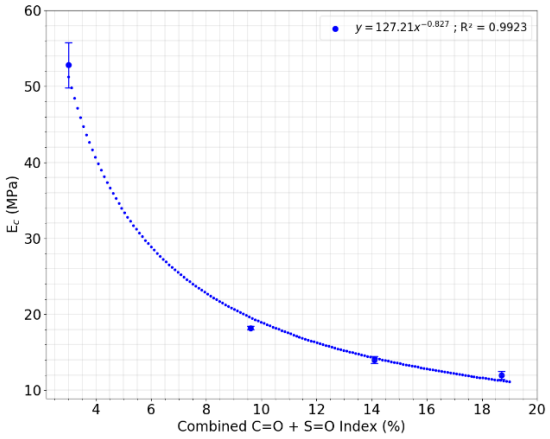

Figure 23. Relation between the crossover modulus E_c for bitumens vs. I_{SO} + I_{CO} index.

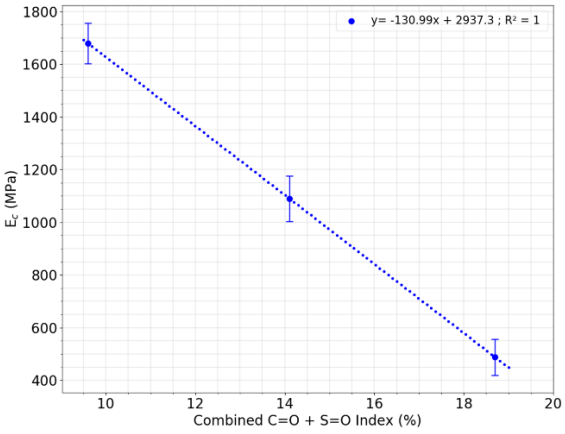

Figure 24. Relation between the crossover modulus Ec for bituminous mixes vs. I_{SO} + I_{CO} index.

The R-value is plotted as a function of the aging duration and combined aging index I_{CO} + I_{SO} for bitumen in Figures 25 and 26, and then for bituminous mixes in Figures 27 and 28. A linear correlation with coefficients of determination R^2 equal to 0.95 and 0.89 can be identified for bitumen. A better linear correlation has been derived for bituminous mixes, with $R^2 \approx 0.99$ for R-value vs. aging time and R^2 = 0.97 for R-value vs. the I_{SO} + I_{CO} index. Other correlations involving bituminous binders can also be found in the literature, e.g. the correlation between R-value and carbonyl index I_{CO}, and the relationship between R-value and viscoelastic transition temperature Tc for binders, as presented by Somé et al. (2023).

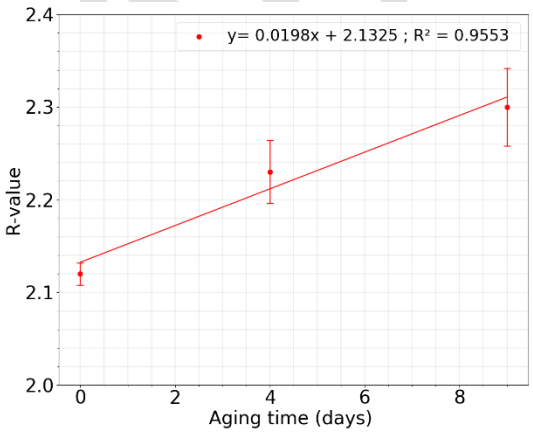

Figure 25. Evolution of bitumens R-values as a function of aging time.

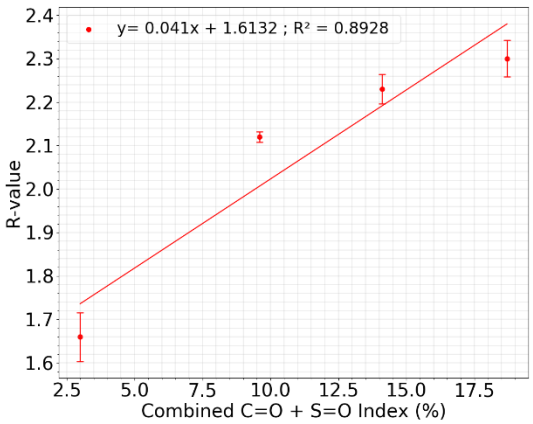

Figure 26. Evolution of bitumens R-values versus aging index (AI = I_{SO} + I_{CO}).

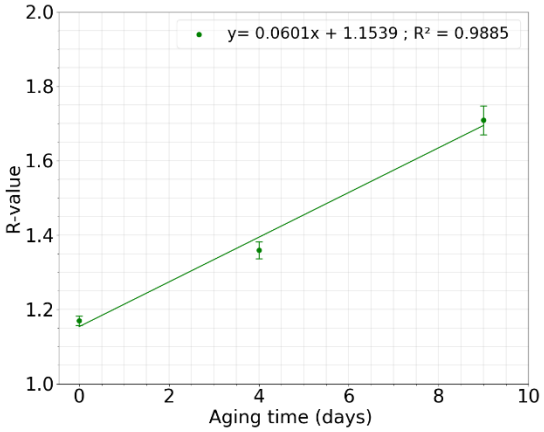

Figure 27. Evolution of mixes R-values as a function of aging time.

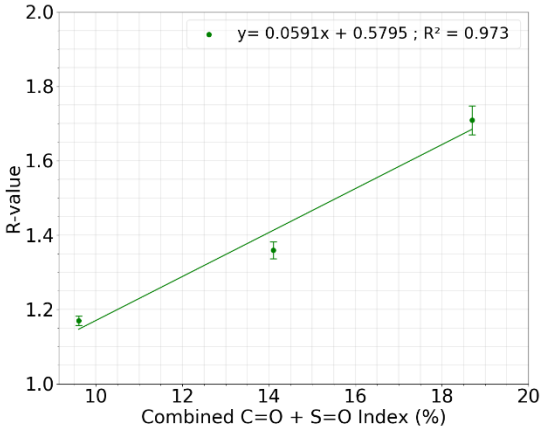

Figure 28. Evolution of mixes R-values versus aging index (AI = ISO + ICO).

Creep-recovery curves yield numerous parameters capable of finely analyzing the behavior of bituminous mixes. We have chosen herein the steady-state creep viscosity η_0 to analyze how mixes age. η_0 corresponds to the equilibrium viscosity when the strain rate becomes constant; it can be calculated as follows (Equation (18)):

$$\eta_0 = \left(\frac{dJ(t)}{dt}\right)^{-1} \tag{18}$$

The steady-state viscosity is defined here as the portion of the curve where $\frac{\Delta\eta_0}{\eta_0} \leq 1\%$. Where $\Delta\eta_0$ is the variation of the strain rate between two-time steps Δt such that $\Delta t = 1s$.

Figure 29 illustrates the evolution of steady-state viscosity as a function of aging time. Let's point out that creep viscosity decreases with increasing temperature and increases with longer aging time. Higher temperatures typically lead to the increased molecular thermal energy of bitumen and reduced flow resistance, which in turn leads to lower viscosity (Abed and Al-Haddad, 2020).

The linear trend in the increase of η_0 highlights the progressive impact of aging on the mechanical response of bituminous mixes. This increase in η_0 is in accordance with the changes in stiffness and creep behavior of the mixes due to aging, as demonstrated in previous work on bituminous concrete cores from road sections (Said, 2005). The evolution of steady-state creep viscosity vs. the sum of the two indices I_{SO} + I_{CO}, as an aging indicator, is displayed in Figure 30. The curves at -5°C, 0°C, 5°C and 10°C all reveal a linear relationship between the two parameters, thus demonstrating a good correlation between creep parameter η_0 and chemical indicator (I_{SO} + I_{CO}). The linear trends under these temperature conditions indicate a significant association between the steady-state creep viscosity and aging effects, as quantified by chemical indicators. These results highlight the relationship between the effects of aging on viscoelastic behavior and the chosen creep indicator, hence demonstrating the reliability of steady-state creep viscosity as a mechanical test indicator for monitoring the aging of bituminous mixes. This relationship is key to understanding how oxidative aging influences mechanical properties over time, in contributing to a global understanding of aging mechanisms in bituminous mixes and providing valuable insight into creep viscosity for non-tested intermediate aging durations.

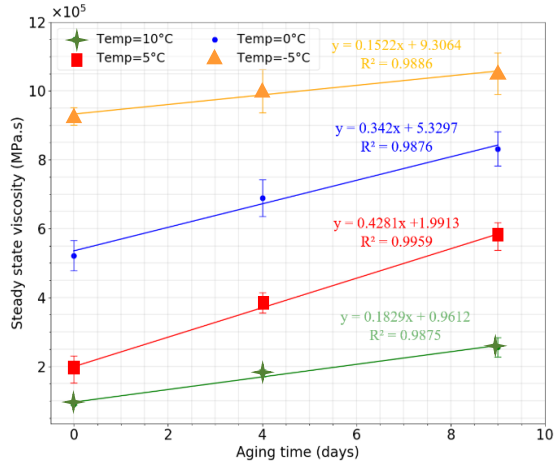

Figure 29. Steady-state creep viscosity vs. aging time.

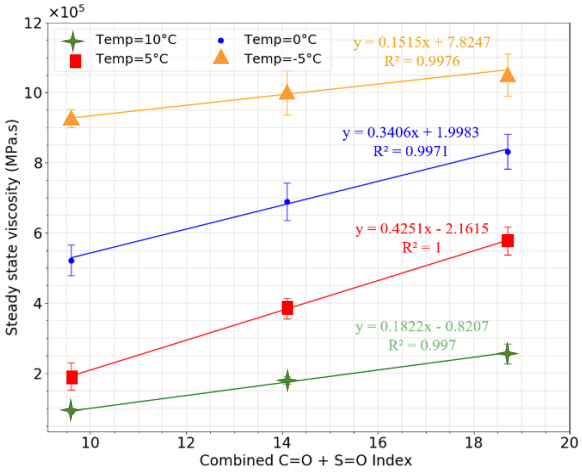

Figure 30. Steady-state creep viscosity vs. ($I_{S=O}$ + $I_{C=O}$).

As mentioned above, the aging of bituminous mixes can be assessed by rheological parameters within the frequency domain or else by creep parameters within the time domain. Both types of parameters have been used to establish correlations with aging indicators, in achieving varying degrees of accuracy (i.e. a strong correlation for steady-state creep viscosity at all temperatures: $R^2 > 0.98$). Nevertheless, the differences between the two approaches need to be reconciled in order to select the most appropriate parameters for aging characterization. Test accuracy is an important parameter for purposes of comparison. The differences between the tensile creep test and the complex modulus generally pertain to the following points: the equation to obtain the resultant value, sensor accuracy, and frame rigidity with respect to bituminous concrete samples. These variables affect the accuracy of the results obtained. For the tensile creep-recovery test, the extensometers used offer high precision, with an error of just ± 0.4 µm to ± 0.5 µm over a measurement length of 100 mm. The precision of steady-state creep viscosity relies on accurately determining the creep compliance rate $\frac{dJ(t)}{dt}$, within the steady-state creep region. This rate corresponds to the slope of the creep curve in this specific region. For instance, at a temperature of 10°C, the standard deviation of the measured steady-state creep compliance rate equals 0.21×10^{-6} ($MPa.s^{-1}$). In the case of complex modulus tests, the standard deviation between measurements at 10°C, 10 Hz is 543 MPa. In addition, the determination of the R-value, used to establish the correlation for the frequency test, also shows a variation that manifests itself in the glass modulus E_g extrapolation, which requires the test to be performed at a very low temperature in order to reach the glass transition region and obtain an accurate extrapolation.

5 Conclusion

The present paper has studied the effect of thermo-oxidative aging in the laboratory on the viscoelastic parameters of both bituminous mixes and binders. The experimental work herein has focused on the mechanical characterization and physicochemical characterization of both aged and non-aged bituminous mixes, as well as on the correlation and comparison of these characterization methods. Simulation based on rheological models was investigated in the context of time-dependent and frequency sweeps, by modeling the creep-recovery test for all aging levels applied. The main conclusions to be drawn are as follows:

- The frequency domain characterization shows that the stiffness moduli of mixes increase with oxidative aging time. Thermo-oxidative aging exerts a significant impact on the physicochemical properties of bitumen through increasing not only asphaltene content but also sulfoxide and carbonyl

indices. Additionally, this enables the establishment of a relationship between the crossover modulus (E_c) and the physicochemical parameters.

- The creep-recovery characteristics of bituminous mixes change with aging, as creep resistance increases. The steady-state creep viscosity has proven to be a relevant indicator of aging, in comparison with the rheological index. A strong correlation between η_0 and $I_{S=0} + I_{C=0}$ was indeed observed.
- Utilization of the same shift factors (a_t) for both complex modulus tests and creep tests reinforces the connection between the viscoelastic properties in both the frequency and time domains. This validation supports the Time-Temperature Superposition Principle for both complex modulus tests and creep tests.
- The prediction of axial strain in creep tests for T0, T4 and T9 bituminous mixes has proven to be successful by employing the complex modulus used in calibrating the Generalized Maxwell and Huet-Sayegh models. The transition from the complex to the time domain has been facilitated through application of the inverse Laplace transform.

In conclusion, the proposed correlations between the index and aging durations, as well as between the rheological and creep properties of aged bituminous mixes, provides an overview of the relevance of using each method when monitoring oxidative aging.

References

Abed, Y. H., & Al-Haddad, A. H. A. (2020). Temperature susceptibility of modified asphalt binders. In IOP Conference Series: Materials Science and Engineering (Vol. 671, No. 1, p. 012121). IOP Publishing. https://doi.org/10.1088/1757-899X/671/1/012121

Airey, G. D., Rahimzadeh, B., & Collop, A. C. (2003a). Viscoelastic linearity limits for bituminous materials. Materials and Structures,36(10), 643–647.doi:10.1007/BF02479495

Airey, G. D., Rahimzadeh, B., & Collop, A. C. (2003b). Linear viscoelastic performance of asphaltic materials. Road Materials and Pavement Design,4(3), 269–292. doi:10.1080/14680629.2003.9689949

Briliak, D., & Remišová, E. (2022). Stiffness modulus of aged asphalt mixtures. Solid State Phenomena, 329, 93-100. https://doi.org/10.4028/p-pc709y

Booij, H. C., & Thoone, G. P. J. M. (1982). Generalization of Kramers-Kronig transforms and some approximations of relations between viscoelastic quantities. Rheologica Acta, 21, 15-24.

Braham, A. F., Buttlar, W. G., Clyne, T. R., Marasteanu, M., & Turos, M. I. (2009). The effect of long-term laboratory aging on asphalt concrete fracture energy. In Asphalt Paving Technology: Association of Asphalt Paving Technologists-Proceedings of the Technical Sessions (Vol. 78, pp. 417-445). Association of Asphalt Paving Technologist.

Buttlar, W. G., Roque, R., & Reid, B. (1998). Automated procedure for generation of creep compliance master curve for asphalt mixtures. Transportation Research Record, 1630(1), 28-36.

Chailleux, E., Ramond, G., Such, C., & de La Roche, C. (2006). A mathematical-based master-curve construction method applied to complex modulus of bituminous materials. Road Materials and Pavement Design, 7(sup1), 75-92. https://doi.org/10.1080/14680629.2006.9690059

Claine Petersen, J. (1998). A dual, sequential mechanism for the oxidation of petroleum asphalts. Petroleum Science and Technology, 16(9-10), 1023-1059. https://doi.org/10.1080/10916469808949823

Cohen, A. M. (2007). Numerical methods for Laplace transform inversion (Vol. 5). Springer Science & Business Media.

Coons, R. F., & Wright, P. H. (1965). An investigation of the hardening of asphalt recovered from pavements of various ages (Master's thesis, Georgia Institute of Technology. Directed by Paul H. Wright.).

Christensen, D. W., & Anderson, D. A. (1992). Interpretation of dynamic mechanical test data for paving grade asphalt cements (with discussion). Journal of the Association of asphalt paving technologists, 61.

Crucho, J., Picado-Santos, L., Neves, J., Capitão, S., & Al-Qadi, I. L. (2020). Tecnico accelerated ageing (TEAGE)–a new laboratory approach for bituminous mixture ageing simulation. International Journal of Pavement Engineering, 21(6), 753-765. https://doi.org/10.1080/10298436.2018.1508845

Daoudi, A., Perraton, D., Dony, A., & Carter, A. (2020). From complex modulus E* to creep compliance D (t): Experimental and modeling study. Materials, 13(8), 1945. https://doi.org/10.3390/ma13081945.

De La Roche, C., & Van de Ven, M. (2009). Development of a laboratory bituminous mixtures ageing protocol. In Advanced Testing and Characterization of Bituminous Materials, Two Volume Set (pp. 347-362). CRC Press.

Dukatz, E. (2015, April). STH 77 Project Objectives. In FHWA Asphalt Mixture ETG meeting.

Durrieu, F., Farcas, F., & Mouillet, V. (2007). The influence of UV aging of a styrene/butadiene/styrene modified bitumen: comparison between laboratory and on site aging. Fuel, 86(10-11), 1446-1451. https://doi.org/10.1016/j.fuel.2006.11.024

EN 12607-1 (2014). Bitumen and bituminous binders - Determination of the resistance to hardening under the influence of heat and air - Part 1: RTFOT method.

EN 14769 (2012). Bitumen and bituminous binders - accelerated long-term ageing conditioning by a pressure ageing vessel (PAV). European Standard.

EN 13108-1 (2017). Bituminous mixtures - Material specifications – Asphalt Concrete.

EN 1426 (2018). Bitumen and bituminous binders - determination of needle penetration. European Standard.

EN 1427 (2018). Bitumen and bituminous binders - determination of the softening point - ring and ball method. European Standard.

EN 12697-33 (2019). Bituminous mixtures - test methods - part 33: roller compactor. European Standard.

EN 12697-26 (2018). Bituminous mixtures - test methods - part 26: Stiffness. European Standard.

FD T66-065 (2018). Bitumen and bituminous binders - Determination of the complex modulus – Elasticimeter

Farrar, M. J., Turner, T. F., Planche, J. P., Schabron, J. F., & Harnsberger, P. M. (2013). Evolution of the crossover modulus with oxidative aging: Method to estimate change in viscoelastic properties of asphalt binder with time and depth on the road. Transportation research record, 2370(1), 76-83. https://doi.org/10.3141/2370-1

Fernández-Gómez, W. D., Vides-Berdugo, A. C., Roncallo-Contreras, S. P., Bautista-Rondón, F., Rondón-Quintana, H. A., & Reyes-Lizcano, F. A. (2016). Effects of environmental aging and ultra violet radiation on asphalt mixture dynamic modulus, permanent deformation and fatigue life. Revista Facultad de Ingeniería Universidad de Antioquia, (80), 89-96. https://doi.org/10.17533/udea.redin.n80a10

Ferry, J. D. (1980). Viscoelastic properties of polymers. John Wiley & Sons.

Glaser, R. R., Schabron, J. F., Turner, T. F., Planche, J. P., Salmans, S. L., & Loveridge, J. L. (2013). Low-temperature oxidation kinetics of asphalt binders. Transportation research record, 2370(1), 63-68. https://doi.org/10.3141/2370-0

Gross, B. (1953). Mathematical structure of the theories of viscoelasticity. Hermann & Cie, Paris.

Guide for mechanistic-empirical design of new and rehabilitated pavement structures. NCHRP 1-37A final report. Transportation Research Board, National Research Council, Washington, D.C. USA, 2004.

Hammoum F., Chailleux E., Nguyen H-N, Erhlacher A., Piau J-M, Bodin D. (2009). Experimental and Numerical Analysis of Crack Initiation and Growth in Thin Film of Bitumen, Road Materials and Pavement Design, 10:1, 39-61.

Hofko, B., Cannone Falchetto, A., Grenfell, J., Huber, L., Lu, X., Porot, L., ... & You, Z. (2017). Effect of short-term ageing temperature on bitumen properties. Road Materials and Pavement Design, 18(sup2), 108-117. https://doi.org/10.1080/14680629.2017.1304268

Kambham, B. S., Ram, V. V., & Raju, S. (2019). Investigation of laboratory and field aging of bituminous concrete with and without anti-aging additives using FESEM and FTIR. Construction and Building Materials, 222, 193-202. https://doi.org/10.1016/j.conbuildmat.2019.06.153

Kandhal, P. S., & Chakraborty, S. (1996). Effect of asphalt film thickness on short-and long-term aging of asphalt paving mixtures. Transportation Research Record, 1535(1), 83-90. https://doi.org/10.1177/0361198196153500111

Kim, J., Sholar, G. A., & Kim, S. (2008). Determination of accurate creep compliance and relaxation modulus at a single temperature for viscoelastic solids. Journal of Materials in Civil Engineering, 20(2), 147–156. https://doi.org/10.1061/(ASCE)0899-1561(2008)20:2(147)

Kim, Y. R., Castorena, C., Elwardany, M., Rad, F. Y., Underwood, B. S., Gundla, A., ... & Glaser, R. R. (2018). Long-term aging of asphalt mixtures for performance testing and prediction.

Lamontagne, J., Durrieu, F., Planche, J. P., Mouillet, V., & Kister, J. (2001). Direct and continuous methodological approach to study the ageing of fossil organic material by infrared microspectrometry imaging: application to polymer modified bitumen. Analytica chimica acta, 444(2), 241-250. https://doi.org/10.1016/S0003-2670(01)01235-1

Lesueur, D., Gérard, J. F., Claudy, P., Létoffé, J. M., Planche, J. P., & Martin, D. (1997). Relationships between the structure and the mechanical properties of paving grade asphalt cements. J. Assoc. Asphalt Paving Techn, 66, 486-507.

Lu, X., & Isacsson, U. (2002). Effect of aging on bitumen chemistry and rheology. Construction and Building materials, 16(1), 15-22.

Lu, X., Redelius, P., Soenen, H., & Thau, M. (2011). Material characteristics of long lasting asphalt pavements. Road materials and pavement design, 12(3), 567-585. https://doi.org/10.1080/14680629.2011.9695261

Lu, X., Talon, Y., & Redelius, P. (2008). 406-001 Aging of bituminous binders–Laboratory tests and field data. In 4th Eurasphalt Eurobitume Congress (pp. 1-12).

Margaritis, A., Soenen, H., Fransen, E., Pipintakos, G., Jacobs, G., & Blom, J. (2020). Identification of ageing state clusters of reclaimed asphalt binders using principal component analysis (PCA) and hierarchical cluster analysis (HCA) based on chemo-rheological parameters. Construction and Building Materials, 244, 118276. https://doi.org/10.1016/j.conbuildmat.2020.118276

Mastoras, F., Varveri, A., van Tooren, M., & Erkens, S. (2021). Effect of mineral fillers on ageing of bituminous mastics. Construction and Building Materials, 276, 122215. https://doi.org/10.1016/j.conbuildmat.2020.122215

Mirwald, J., Nura, D., & Hofko, B. (2022). Recommendations for handling bitumen prior to FTIR spectroscopy. Materials and Structures, 55(2), 26. https://doi.org/10.1617/s11527-022-01884-1

Mirwald, J., Maschauer, D., Hofko, B., and Grothe, H. (2020). Impact of reactive oxygen species on bitumen aging - The Viennese binder aging method. Construction and Building Materials, 257:119495. https://doi.org/10.1016/j.conbuildmat.2020.119495

Maschauer, D., Steiner, D., Mirwald, J. et al. Chemical and mechanical analysis of VAPro-aged asphalt binders from different crude oil sources. Mater Struct 56, 168 (2023). https://doi.org/10.1617/s11527-023-02249-y

Mohammad, L. N., Kim, M., Raghavendra, A., & Obulareddy, S. (2014). Characterization of Louisiana asphalt mixtures using simple performance tests and MEPDG (No. FHWA/LA. 11/499). Louisiana. Dept. of Transportation and Development.

Mollenhauer, K., Mouillet, V., (2011) Re-road – End of Life Strategies of Asphalt Pavements. European Commission DG Research

Mouillet, V., Farcas, F., Battaglia, V., Besson, S., and C. Petiteau, F. L. (2010). Identification and quantification of bituminous binder's oxygenated species. Analysis by Fourier Transform InfraRed spectroscopy. Testing method LPC no69 (2010), pages 1–9.

Olard, F. & Di Benedetto, H. (2003). General 2s2p1d model and relation between the linear viscoelastic behaviours of bituminous binders and mixes. Road Materials and Pavement Design, 4 Issue 2:185–224. https://doi.org/10.1080/14680629.2003.9689946

Omranian, S. R., Hamzah, M. O., Valentin, J., & Hasan, M. R. M. (2018). Determination of optimal mix from the standpoint of short term aging based on asphalt mixture fracture properties using response surface method. Construction and Building Materials, 179, 35-48. https://doi.org/10.1016/j.conbuildmat.2018.05.078

Piérard, N., Vanelstraete, A., Développement d'une méthode d'essai pour vieillir de manière accélérée les enrobés bitumineux en laboratoire, XXIème Congrès Belge de la Route, Gent, 22-25 septembre 2009, paper I.1.9.

Rad, F. Y., Elwardany, M. D., Castorena, C., & Kim, Y. R. (2017). Investigation of proper long-term laboratory aging temperature for performance testing of asphalt concrete. Construction and Building Materials, 147, 616-629.

Said, S. F. (2005). Aging effect on mechanical characteristics of bituminous mixtures. Transportation Research Record, 1901(1), 1-9. https://doi.org/10.1177/0361198105190100101

Sayegh, G. (1965). Contribution à l'étude des propriétés viscoélastiques des bitumes purs et des bétons bitumineux. PhD, University Paris 6.

Shell Pavement Design Manual-Asphalt Pavements and Overlays for Road Traffic, Shell International Petroleum, London, U.K., 1978.

Sirin, O., Paul, D. K., & Kassem, E. (2018). State of the art study on aging of asphalt mixtures and use of antioxidant additives. Advances in Civil Engineering, 2018. https://doi.org/10.1155/2018/3428961

Soleimani, P. (1967). Etude sur le comportement viscoélastique des matériaux bitumineux par la méthode de fluage. Rheologica Acta, 6, 222-239. https://doi.org/10.1007/BF01976439

Somé, S. C., Barthélémy, J. F., Mouillet, V., Hammoum, F., & Liu, G. (2022). Effect of thermo-oxidative ageing on the rheological properties of bituminous binders and mixes: Experimental study and multi-scale modeling. Construction and Building Materials, 344, 128260. https://doi.org/10.1016/j.conbuildmat.2022.128260

Somé, S. C., Kouevidjin, A. B., Mouillet, V., Feeser, A., Barthélémy, J. F., & Ben Dhia, H. (2023). Evaluation of effects of short and long-term thermo-oxidative aging on chemo-rheological and mechanical properties of asphalt concretes. Road Materials and Pavement Design, Vol 24 Issue 12, 1-30. https://doi.org/10.1080/14680629.2023.2173083

Sreeram, A., Masad, A., Nia, Z. S., Maschauer, D., Mirwald, J., Hofko, B., and Bhasin, A. (2021). Accelerated aging of loose asphalt mixtures using ozone and other reactive oxygen species. Construction and Building Materials, 307:124975. https://doi.org/10.1016/j.conbuildmat.2021.124975

Tabasi, E., Zarei, M., Alaei, H., Tarafdar, M., Alyousuf, F. Q. A., & Khordehbinan, M. W. (2023). Evaluation of long-term fracture behavior of hot mix asphalt modified with Nano reduced graphene oxide (RGO) under freeze–thaw damage and aging conditions. Construction and Building Materials, 374, 130875. https://doi.org/10.1016/j.conbuildmat.2023.130875

Tai Nguyen, H. T., Nguyen, D. L., Tran, V. T., & Nguyen, M. L. (2022). Finite element implementation of Huet-Sayegh and 2S2P1D models for analysis of asphalt pavement structures in time domain. Road Materials and Pavement Design, 23(1), 22-46. https://doi.org/10.1080/14680629.2020.1809501

Tai Nguyen, H. T., Do, T. T., Tran, V. T., Phan, T. N., Pham, T. A., & Nguyen, M. L. (2021). Determination of creep compliance of asphalt mixtures at intermediate and high temperature using creep-recovery test. Road Materials and Pavement Design, 22(sup1), S514-S535. https://doi.org/10.1080/14680629.2021.1908407

TS 12697-52 (2017). Bituminous mixtures - test methods - part 52: Conditioning to address oxidative ageing. European Standard.

Wang, Z., & Ye, F. (2020). Experimental investigation on aging characteristics of asphalt based on rheological properties. Construction and Building Materials, 231, 117158. https://doi.org/10.1016/j.conbuildmat.2019.117158

Wang, Z., & Ye, F. (2020). Experimental investigation on aging characteristics of asphalt based on rheological properties. Construction and Building Materials, 231, 117158. https://doi.org/10.1016/j.conbuildmat.2019.117158

Wen, H., Liu, F., & Cheng, J. (2016). Development of Oxidation Kinetics Models for Rheological and Damage Properties Based on "In-Service" Asphalt Binders. Journal of the Association of Asphalt Paving Technologists, (85).

Witczak, M. W., Von Quintus, H. L., & Schwartz, C. W. (1997). Superpave support and performance models management: Evaluation of the SHRP performance models system. In Eighth International Conference on Asphalt PavementsFederal Highway Administration (No. Volume III).

Xiao, F., Amirkhanian, S. N., Karakouzian, M., & Khalili, M. (2015). Rheology evaluations of WMA binders using ultraviolet and PAV aging procedures. Construction and Building Materials, 79, 56-64. https://doi.org/10.1016/j.conbuildmat.2015.01.046

Yang, Z., Zhang, X., Zhang, Z., Zou, B., Zhu, Z., Lu, G., ... & Yu, H. (2018). Effect of aging on chemical and rheological properties of bitumen. Polymers, 10(12), 1345. https://doi.org/10.3390/polym10121345

Zhang, R., Sias, J. E., & Dave, E. V. (2022). Evaluation of the cracking and aging susceptibility of asphalt mixtures using viscoelastic properties and master curve parameters. Journal of Traffic and Transportation Engineering (English Edition), 9(1), 106-119. https://doi.org/10.1016/j.jtte.2020.09.002

Zhang, X., Han, C., Zhou, X., Otto, F., & Zhang, F. (2021). Characterizing the diffusion and rheological properties of aged asphalt binder rejuvenated with bio-oil based on molecular dynamic simulations and laboratory experimentations. Molecules, 26(23), 7080. https://doi.org/10.3390/molecules26237080

Zhang, W., Bahadori, A., Shen, S., Wu, S., Muhunthan, B., & Mohammad, L. (2018). Comparison of laboratory and field asphalt aging for polymer-modified and warm-mix asphalt binders. Journal of Materials in Civil Engineering, 30(7), 04018150. https://doi.org/10.1061/(ASCE)MT.1943-5533.0002354

Zhang, D., Birgisson, B., Luo, X., & Onifade, I. (2019). A new short-term aging model for asphalt binders based on rheological activation energy. Materials and Structures, 52, 1-22. https://doi.org/10.1617/s11527-019-1364-7